

Estimating the roughness of muddy beds

H.J. Speerstra

A study based on in-site measurements and numerical modeling



Estimating the roughness of muddy beds

by

H.J. Speerstra

to obtain the degree of Master of Science
at the Delft University of Technology,
to be defended publicly on Tuesday June 18, 2018 at 16:00.

Supervisor:	Prof. dr. ir. P.M.J. Herman,	TU Delft and Deltares
Thesis committee:	dr. ir. D.S. van Maren,	TU Delft and Deltares
	ir. T.J. Zitman,	TU Delft
	MSc. I. Colosimo,	TU Delft

An electronic version of this thesis is available at <https://repository.tudelft.nl/>.

Preface

This research report is carried out in order to finish the Master Hydraulic Engineering at Delft University of Technology. It focuses on the bed roughness estimation of muddy beds by using a data set and numerical modeling.

The dataset used in this thesis is collected by Irene Colosimo. She has done a lot of hard work to get this data and I want to thank her for that. I would also like to thank her for all the useful and stimulating talks we had together. She gave me the opportunity to help with fieldwork and I would like to thank her and Bram van Prooijen for the great experience they gave me and wonderful days during the fieldwork.

Part of this research was conducted at Deltares. I am grateful for the workspace and knowledge Deltares provided me to bring this thesis to a good result. I would like to thank Bas van Maren for the helpful and clarifying talks and the useful contacts he made for me at Deltares. Also many thanks to Peter Herman for helping me with the statistical models used in the thesis and guiding me in the right direction towards the end of my thesis. I would also like to thank Han Winterwerp for providing and explaining the numerical model used in this thesis.

All in all, I would like to thank each member of the graduation committee formed by prof. dr. ir. P.M.J. Herman, dr. ir. D.S. van Maren, ir. T.J. Zitman and MSc. I. Colosimo. Their professional guidance, feedback and enthusiastic support helped me during the entire project.

Many thanks goes out to my sister Femke Speerstra for helping me with textual and grammatical improvement of the report.

I would also like to thank all colleague students and friends that supported and motivated me and my family for always supporting and encouraging me throughout my education.

*H.J. Speerstra
Delft, June 2018*

Abstract

Bed roughness is an important parameter for the prediction of sediment transport as well as calculating flow conditions near the bed. Numerical models are extensively used to make these predictions. In these models it is fundamental to have proper values for bed roughness. The bed roughness is being estimated using a dataset from an ongoing pilot project in the Dutch western Wadden Sea. This dataset consists of 40 days of velocity measurements using ADV (8 Hz) and ADCP (1 Hz) instruments and concentration of SPM measurements using OBS instruments.

To estimate the bed roughness, the dataset is analyzed using four methods for calculating the bed shear stress. The logarithmic profile, turbulent kinetic energy, vertical turbulent kinetic energy and the Reynolds stress method.

The data has been processed and averaged per tidal phase, so statistical analysis can be applied to it. From this analysis, it is found that the concentration of SPM increases at 6 cm with increasing wind speed. As a result of this increasing of SPM the bed roughness also increases. This leads to the hypothesis that suspended sediment makes the bed rougher, and is not primarily governed by horizontal advection but also local resuspension.

A 1DV numerical model is used in which horizontal advection is excluded to test this hypothesis. Simulations are performed with stationary boundary conditions, using combinations of water depth (0.2 to 2.8 m) and velocities (5 cm/s to 70 cm/s). These simulations are imposed with an initial homogeneous concentration. For every combination, the concentration is increased gradually until the concentration profile becomes L-shaped.

Besides simulations with stationary conditions, timeseries of water depth and velocity are used to simulate one tidal cycle.

All simulations performed with this numerical model do not take wind and waves into account and water-bed exchange is excluded.

From the simulations with stationary boundary conditions the roughness is calculated using the LP method. It is found that bed roughness increases with increasing initial homogeneous concentration. From the simulation of one tidal cycle, it is found that the roughness increases towards the turn of the tide. After the turning of the tide, the concentration profile becomes L-shaped, and the roughness is decreased. The concentration profile becomes homogeneous again after a certain threshold of velocity and waterdepth and at the same time the roughness increases again. During a tidal cycle, it is possible to have a collapsed concentration profile, which indicates a lower bed roughness and thus a smoother bed.

Contents

Preface	iii
Abstract	v
1 Introduction	1
1.1 Problem formulation	1
1.2 Research goal	2
2 Research approach	5
2.1 Study area	5
2.1.1 Instrumentation setup	6
2.1.2 Data transformation from instruments	7
2.2 Methods for calculating bed shear stress	11
2.2.1 Boundary layer theory	11
2.2.2 Log Profile (LP)	14
2.2.3 Reynolds Stress (RS)	14
2.2.4 Turbulent Kinetic Energy (TKE)	15
2.2.5 Vertical Turbulent Kinetic Energy (TKE _v)	15
2.3 Data analysis	15
2.3.1 Bed shear stress using first momentum methods	16
2.3.2 Bed shear stress using second momentum methods	17
2.3.3 Bed roughness parameters	17
2.3.4 Tidal reversal	18
2.3.5 Tidal analysis	19
2.3.6 Statistical analysis	20
2.4 Modeling	21
2.4.1 Model description	21
2.4.2 Simulations with stationary boundary conditions	21
2.4.3 Simulations with transient boundary conditions	22
2.4.4 Roughness determination from model results	22
3 Results	23
3.1 Data analysis	23
3.1.1 Description of observations	23
3.1.2 Bed shear stress calculations	26
3.1.3 Tide phase averaged roughness	27
3.1.4 Statistical analysis	29
3.2 Modeling	32
3.2.1 Stationary simulation with $h = 1.6$ m and 0.25 m/s	32
3.2.2 Fluid mud formation for stationary conditions	33
3.2.3 Roughness calculation for simulation with stationary conditions	35
3.2.4 Simulations with transient conditions	38
4 Discussion	41
5 Conclusions	43
6 Recommendations	45
A Statistical analysis	47
B Simulations with stationary boundary conditions	57
Bibliography	63

Introduction

1.1 Problem formulation

The bed roughness is one of the important parameters for the prediction of sediment transport as well as defining flow conditions at the sediment-water interface. Nowadays, numerical models are extensively used for making predictions of transport of sediment. The roughness length (z_0) or bed roughness (Nikuradse roughness $k = 30z_0$) is one of the key parameters in such models to determine the bottom boundary conditions for the flow equations. A fixed value is typically used for the roughness which may in reality not always be the case. For instance, temporal variations in bed roughness may be present leading to wrong predictions.

The bed roughness is, in fact, a schematization of several physical processes in a thin layer close to the bed. It is a function of physical grain composition at the water-sediment interface (k_{grain}), hydrodynamic form drag due to bedforms (k_{drag}) and sediment transport near the bed ($k_{sediment}$). The total bed roughness can be written as $k_b = k_{grain} + k_{drag} + k_{sediment}$. When both the form drag and sediment movement are insignificant, the roughness length z_0 is only a function of the physical grain composition and should remain constant when the sediment characteristics do not change.

The fluid motion flowing over the seabed undergoes resistance due to the bed roughness, This causes a shear effect called the bed shear stress which can be parameterized by the bed roughness. So, bed shear stress and bed roughness are related. Methods exist to determine the bed shear stress from in-site measurements, for instance, based on the logarithmic-profile or the turbulent kinetic energy which arises from the turbulent flow caused by the bed.

When the roughness length, z_0 , varies this can be caused by the contribution of form drag and sediment transport to the total bed roughness. In other words, the fluid-sediment interaction can cause the bed to be moveable, and bedforms can be created, which act as a roughness to the flow. The dimensions of the bed forms, which are essential for the actual roughness, are influenced by currents and waves. According to Houwman and van Rijn (1999), an increase in energy conditions above a certain level, flattens the bedforms, and large sediment concentrations are generated. This acts as additional friction to the flow and consequently increased roughness value Grant and Madsen (1982). Houwman and van Rijn (1999) investigated the possibility to model the apparent bed roughness in the presence of currents and waves using a 1DV model. The model was implemented with combinations of bedform models and wave-current models to calculate near-bed velocities. Reasonable results were found, comparing measured and predicted velocities.

Lacy et al. (2005) investigated the temporal variation of the hydrodynamic roughness using velocity profiles in the bottom boundary layer measured with high-resolution acoustic Doppler profiler (PCADP). The study was performed for a site with energetic waves and medium-to-fine sand. Bottom roughness is rarely determined for sites with such conditions. The friction velocity, u_{*c} , due to currents and the apparent bottom roughness, z_{0a} was determined from the profiles using the law of the wall. The bottom roughness, k_b , was estimated using the Grant-Madsen model for wave-current interaction. Resulting values for k_b vary over 3 orders of magnitude (from 1×10^{-1} to 1×10^{-4} m) and they vary inversely with wave orbital diameter. Lacy et al. (2005) suggest making use of time-varying bottom roughness to improve the accuracy of sediment transport models significantly. Lacy et al. (2005) also estimated bedform height from k_b and was consistent with predictions from empirical models and bedforms from sonar imaging.

Cheng et al. (1999) also investigated the bed roughness like Lacy et al. (2005) using broadband acoustic current profilers. The difference with Lacy et al. (2005) is that the bed roughness is evaluated in 24-hour periods and the velocity profile time series are independently analyzed by flooding and ebbing periods. It is found that the estimated values of z_0 and u_* for flooding and ebbing are different and are caused by tidal current flood-ebb inequality. Two regimes of z_0 as a function of a reference velocity were visible. For velocities higher than 25-30 cm/s the $\ln z_0$ is inversely proportional to the reference velocity. The cause of the reduction of roughness length is hypothesized as sediment erosion due to intensifying tidal current and thereby reducing bed roughness. For velocities below 25 cm/s the relation between roughness length and the reference velocity is less pronounced. Cheng et al. (1999) hypothesized that this could be due to sediment deposition.

In this study, the variability in the bed roughness is being evaluated per tidal phase using a dataset together with a numerical model. The in-site measurements are gathered from an ongoing pilot project in the Dutch western Wadden Sea. The purpose of this project is to use dredged bed material from the port of Harlingen and re-use it for ecological purposes. The measurements obtained are conducted using instruments mounted on a frame. These frames are located on an intertidal mudflat close to the port of Harlingen as illustrated in fig. 1.1.

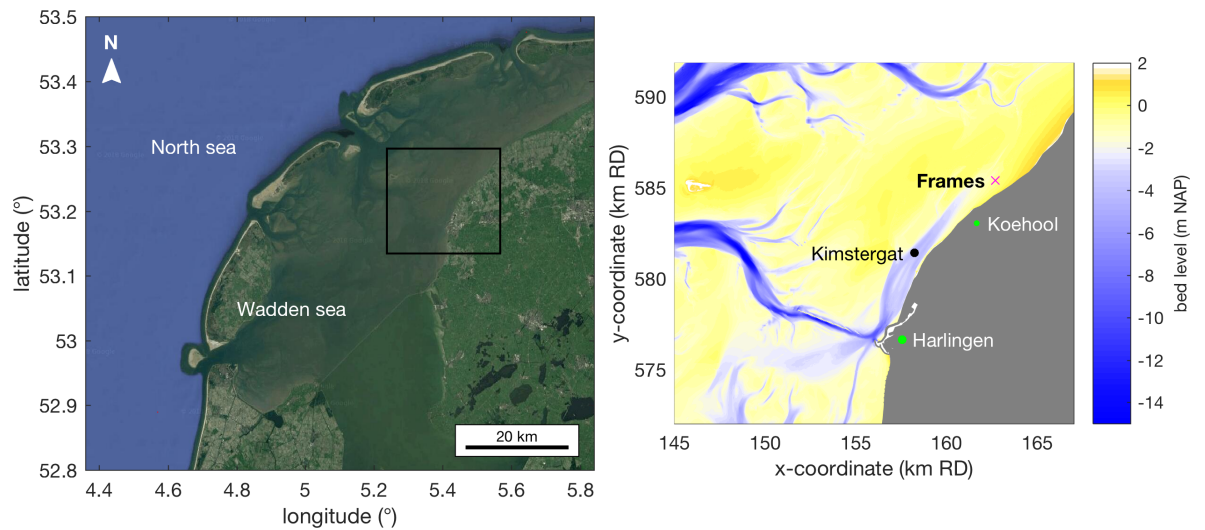


Figure 1.1 Location of the mud motor in the western wadden sea. Kimstergat is the channel and the mudflat is at the location of the frames. The flood direction is towards north-east and ebb is towards south-west.

1.2 Research goal

In this thesis variability in bed roughness is being estimated and investigated. And which mechanism drives this variability.

Possible mechanisms for the variation in bed roughness considered in the present study are illustrated in fig. 1.2.

1. Fine sediment normally on the bed is being suspended during energetic hydrodynamic conditions, leaving rougher material left on the bed (left in fig. 1.2)
2. An irregular bed is being exposed during energetic hydrodynamic conditions (right in fig. 1.2). This mechanism could be further explained by a highly concentrated suspension of fine sediment particles - fluid mud - filling the irregular bed to form a smooth bed. This layer could disappear by either local resuspension or horizontal advection. Winterwerp (2001) describes the observation that can be made when a fluid mud layer is formed. The emphasis in this thesis lies on the first criterium.
 - A collapse in the concentration profile going from a Rousean concentration profile to a fluid mud layer.

- The eddy diffusivity in the upper part of the water column collapses as a result of damping effect (induced by buoyancy terms in the turbulent energy equation), although the profile can be restored a bit from turbulence produced by the shear flow in the water column.
- A decrease in bed shear stress, hence u_*

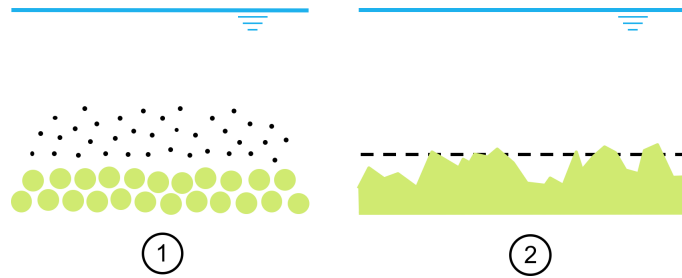


Figure 1.2 Hypothetical mechanisms causing variations in bed roughness

To achieve the research goals, the dataset described earlier will be analyzed by calculating bed roughness using the bed shear stress methods. Statistical analysis will be applied to the results of the data analysis. The outcome of both analyses will be further investigated through 1DV numerical modeling. Chapter 2 will explain the research approach. The dataset of the pilot project is discussed as well as the numerical model. Chapter 3 will present the results of this study followed by the conclusions in chapter 5 and recommendations in chapter 6.

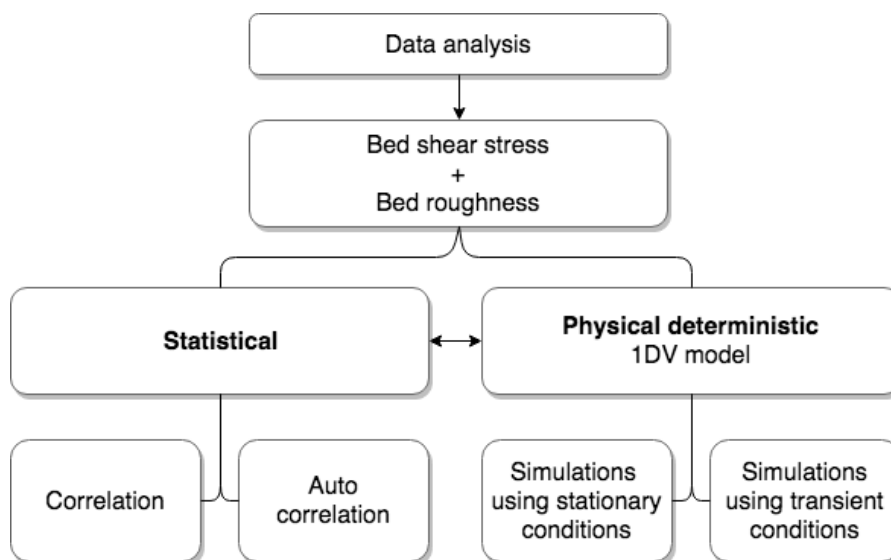
2

Research approach

This chapter describes the components of the research approach which is followed to answer the research goal and question. This research approach can be divided into a data analysis part and a numerical modeling part.

As described in the introduction, a dataset is used from an ongoing pilot project in the Dutch western Wadden Sea. From this data set, the bed shear stress will be calculated using four methods. Statistical analysis will be performed on the data from the dataset together with meteorological information. The outcome and hypothesis arising from this analysis will be further investigated using a physical deterministic approach utilizing a 1DV numerical model. The numerical model will be used to simulate two types of simulations, one where stationary boundary conditions are applied and one where transient boundary conditions are applied. The diagram in chapter 2 gives an overview of the approach.

The following sections will elaborate further on the data analysis and the modeling approach.



After this chapter, the results for both parts are presented.

2.1 Study area

A field campaign in the spring of 2016 is conducted in the western Wadden Sea. The western Wadden sea is part of the Wadden sea stretching from Denmark all the way to the Netherlands. The mud motor project is located in the Vlie tidal basin in the western Wadden Sea.

The field campaign is conducted by placing two frames equipped with measurement instruments. These frames are located at a tidal flat ten km northwards of Harlingen adjacent to the coast close to the city of Koehool, see fig. 2.1.

The shallow character of the Wadden sea forces the port of Harlingen to dredge the harbor and the channels continuously. Yearly an amount of 1.3×10^6 m³ of mud and sand is dredged and deposited

at a designated area in the Wadden Sea, in the vicinity of the harbor. It is one of the most impacting activities caused by the port of Harlingen in the Wadden Sea area. Dredging and disposal of silt and sand on other locations result in significant amount of suspended sediment making the water murky, leading to less sunlight penetrating the water affecting the sea life. Primarily the production of plankton which is, in turn, the staple food source for shrimp and fish. This production is highest during spring and summer; therefore the sea life will benefit from limiting the amount of dredging during these seasons (Baptist, 2017).

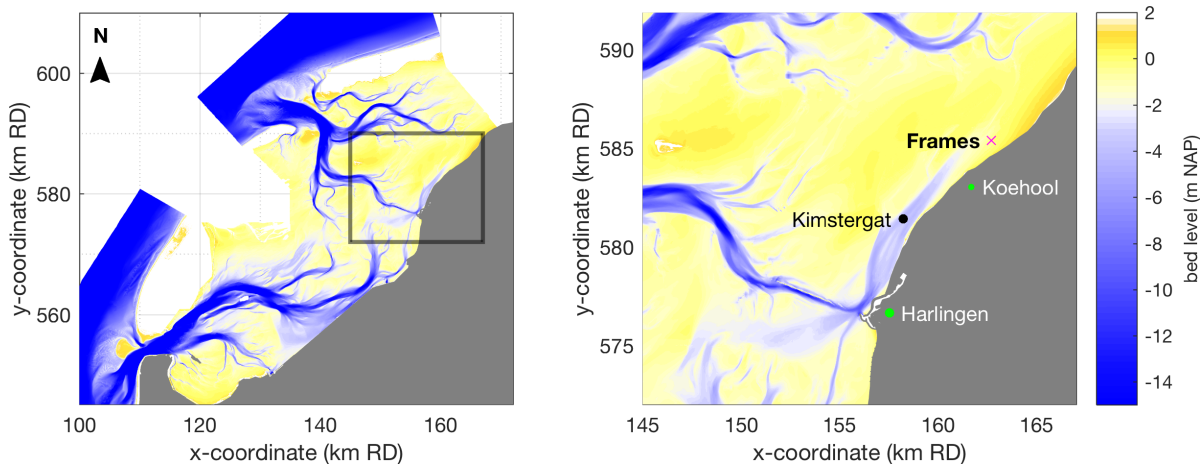


Figure 2.1 Location of the mud motor in the western wadden sea. Kimstergat is the channel and the mudflat is at the location of the frames. The flood direction is towards north-east and ebb is towards south-west.

2.1.1 Instrumentation setup

The field campaign is conducted in spring 2016 from 14th April till the end of may. Two frames are located at the mudflat which is 900 m apart. The frames are aligned such that they are more or less perpendicular to the coastline, see fig. 2.5. The more offshore frame recorded a maximum waterdepth of 2.625 m and the onshore frame measured a maximum waterdepth of 1.87 m. At these two frames instruments were mounted which measure currents, pressure and turbidity.

Three type of instruments can be distinguished: Acoustic Doppler Velocimeter (ADV), Acoustic Doppler Current Profiler (ADCP) and Optical Backscatter (OBS). All instruments are measuring according to the ENU coordinate system (east-north-up).

Per frame two ADV instruments were used to measure the 3D velocity at a high sampling frequency of 8 Hz. One ADV measured continuously. The other ADV measures in bursts mode, meaning that for a specified period (burst duration) measurements are performed followed by a period of no measurements (burst interval). For the offshore frame, the ADV measuring in burst mode had a burst duration of 10 min with an interval of 10 min between the bursts. For the onshore frame, the burst duration was 15 min and the burst interval 5 min. Besides velocity, the pressure is measured from which wave characteristics can be deduced. The ADV measures in burst mode also retrieves the distance from the probe to the bottom for each burst.

Turbidity is measured at each frame using two OBS instruments per frame. Similar to the ADV instruments, there is one measuring continuously and one measuring in bursts. The turbidity signal is converted to a suspended sediment concentration (SSC) using calibration curves from sediment samples.

3D current velocity profiles were measured using one ADCP per frame. Both measure in burst intervals of 10 min with a sampling frequency of 1 Hz.

Meteorological data is obtained from KNMI (Noorden Balgen station) from 12th April 2016 to 27th may 2016 with time intervals of 10 minutes. For each interval, the wind speed and wind direction are provided.

For the present analysis, the instruments from the offshore frame are used because they are fewer moments out of the water and therefore have more data.

In table 2.1 an overview is given for the settings of the instruments installed on the frames.

Table 2.1 Instruments mounted on the two frames for the field campaign conducted in spring 2016. ADCP instruments measure at multiple equidistant heights from the bed with 50 mm between the points. Instruments in burst mode measure in intervals of 10 min

Instrument	Frequency	Distance above bed	Measuring period
<i>Frame 1 (off-shore)</i>			
ADV1	8 Hz, continuous	20 cm	14-Apr till 26-May (42 days)
OBS3	8 Hz, continuous	6 cm	
ADV3	8 Hz, burst	11 cm	14-Apr till 27-May (43 days)
OBS1	8 Hz, burst	11 cm	
ADCP2	1 Hz, burst	16 heights from 20 to 100 cm	14-Apr till 27-May (43 days)
<i>Frame 2 (on-shore)</i>			
ADV2	8 Hz, continuous	10 cm	14-Apr till 13-May (29 days)
ADV4	8 Hz, burst	5 cm	14-Apr till 17-May (33 days)
ADCP1	1 Hz, burst	11 heights from 56 to 111 cm	14-Apr till 27-May (43 days)
OBS			
OBS			

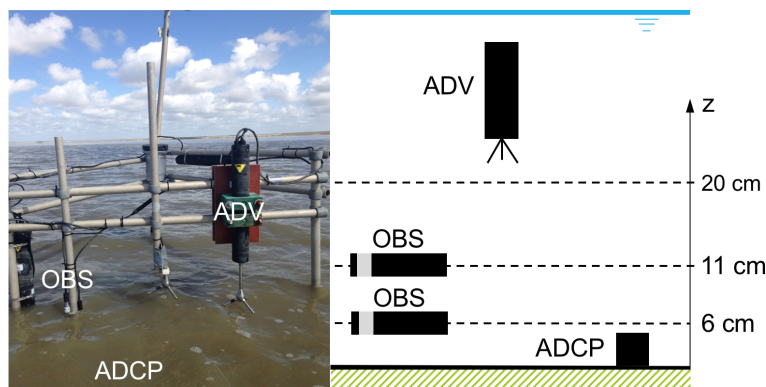


Figure 2.2 Schematic representation of the instruments at the offshore frame.

2.1.2 Data transformation from instruments

ADV

Three datasets of the ADV instruments can be distinguished: 3D velocities, wave characteristics and bed level changes. The pressure measured by the ADV is the total pressure consisting of water pressure and air pressure. The water depth is computed by subtracting the air pressure from the total pressure and then wave characteristics are computed using the zero-crossing method on the processed water depth signal. The latter is only applied for ADV instruments measuring continuously. Bed level changes can be determined from the distance from the probe to the bottom. This is done and only applicable to the ADV measuring in burst mode. Before further analysis can be performed on the data, low-quality signals need to be filtered out. Low-quality data is indicated by low correlation, amplitude and/or signal-to-noise ratios (SNR). This can be the case when the instrument is emerged and exposed to air instead of water. The ADV used in the present analysis is measuring at a distance of 20 cm from the bed. Typically the data is assumed to be of good quality when the correlation $\geq 70\%$, the amplitude ≥ 100 counts and the SNR ≥ 20 dB, see fig. 2.3

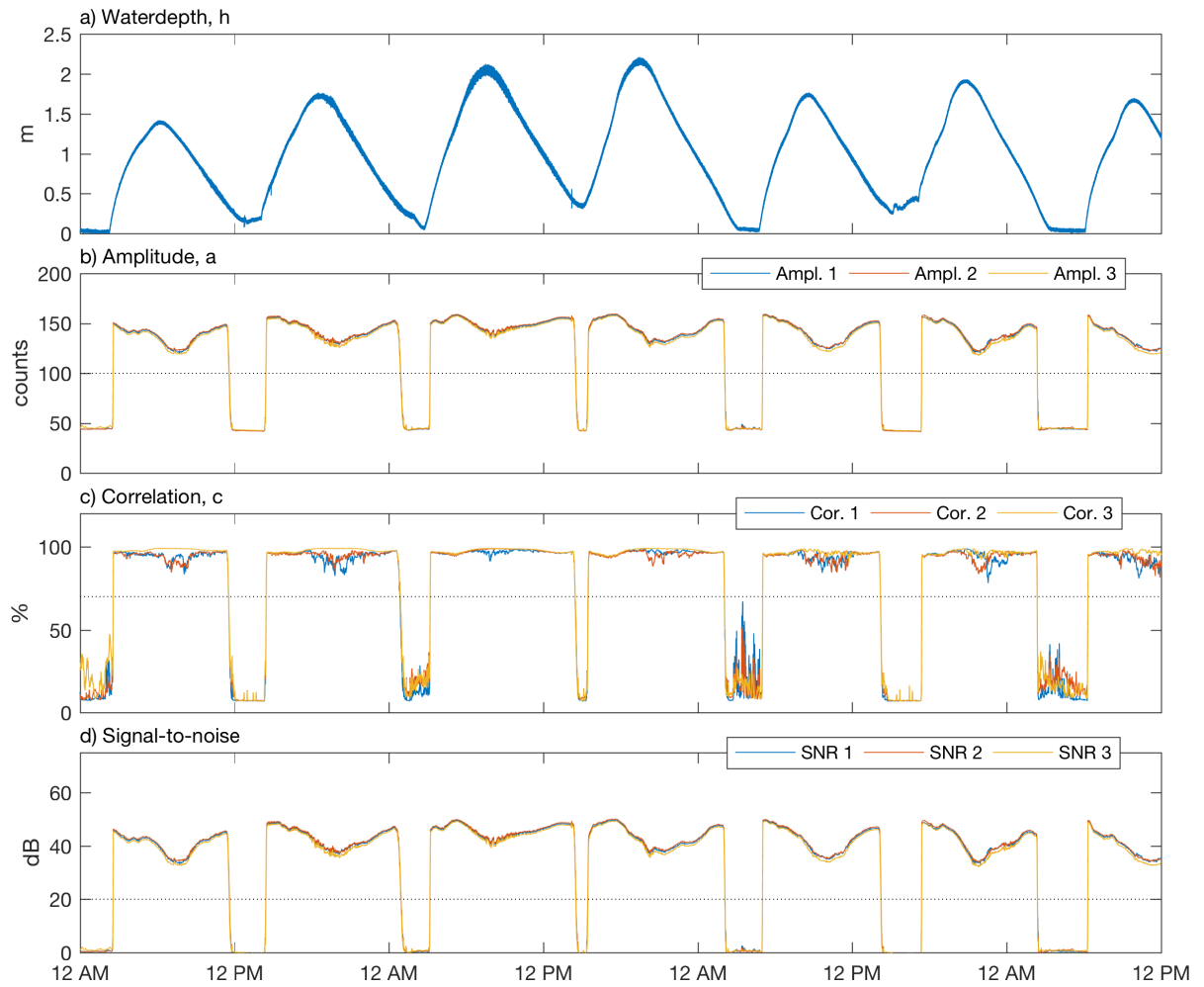


Figure 2.3 Acoustic parameters from ADV instrument at off-shore frame measuring in continuous mode (time series from 2nd May to 5th May). When air replaces the medium in which the device is placed, the acoustic parameters (a, c and SNR) become low. Data above the dotted lines indicate signals with good quality.

ADCP

The ADCP gives a dataset of three-dimensional velocities at multiple heights above the bed. The data is filtered using a similar approach as for the ADV instruments. The criterion for good quality data is a correlation of at least 70 % and a minimum amplitude of 100 counts. Figure 2.4 gives the acoustic amplitudes and beam correlations at two different heights above the bed. The ADCP on the off-shore frame measures at 16 levels above the bed in bins of 5 cm measuring from 20 cm to 100 cm above the bed. The onshore ADCP measures at 11 levels above the bed in bins of 5 cm from 56 cm to 111 cm.

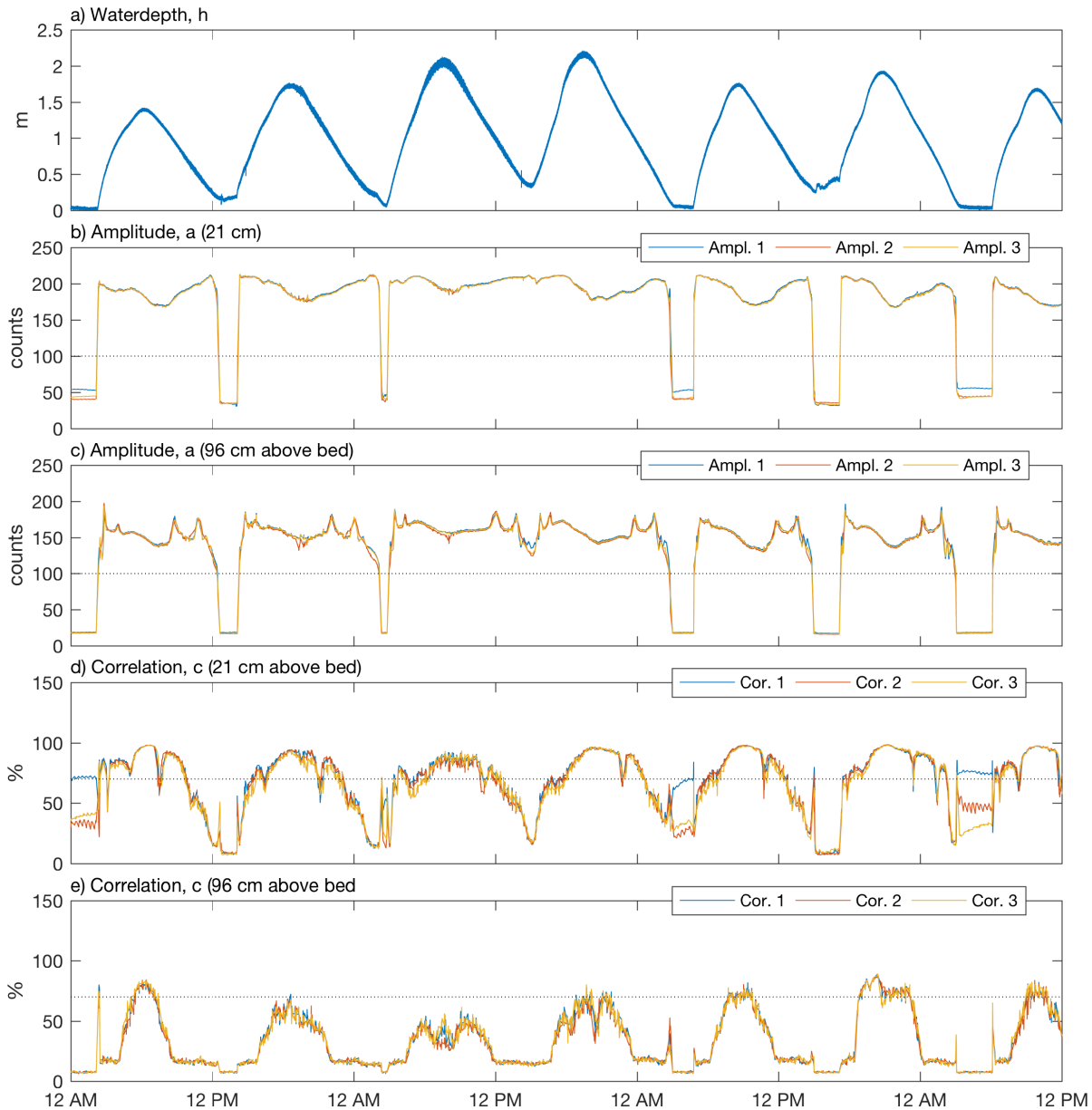


Figure 2.4 Acoustic parameters from ADCP instrument at off-shore frame measuring in burst mode (time series from 2nd May to 5th May). When air replaces the medium in which the device is placed, the acoustic parameters (a and c) become low. This happens more often for data measured higher in the water column. Data above the dotted lines indicate signals with good quality.

OBS

The OBS instruments measure turbidity which is converted to suspended sediment concentrations using calibration curves of the OBS instruments. How to perform the calibration is not discussed here as well

as the calibration curves.

Coordinate system

All instruments measure according to the ENU coordinate system. The north and east directions of this coordinate system do not coincide with the alongshore and cross-shore direction (see fig. 2.5 for the orientation of the coastline). Therefore, this coordinate system is rotated to align with the tidal flow direction in the channel which is approximately alongshore. Thus, all datasets containing directions are rotated by an angle of 45 degrees (CCW) in the horizontal plane, see fig. 2.5.

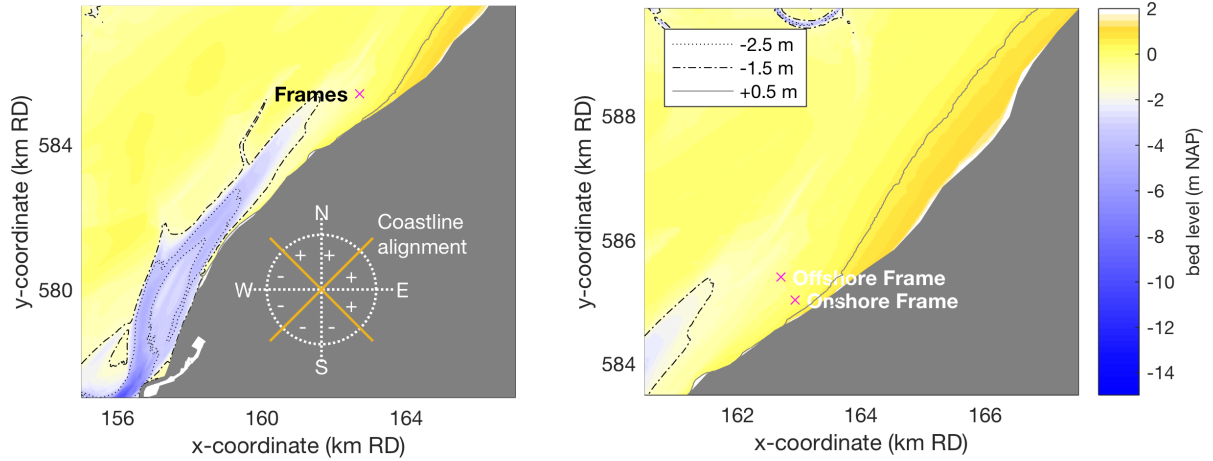


Figure 2.5 Detailed bathymetry of Kimstergat channel and Koehool mudflat. The frames are located at the Koehool mudflat.

2.2 Methods for calculating bed shear stress

This section sums up the bed shear stress methods along with the underlying theory of the methods. Furthermore, a brief description of the physical processes on intertidal flats are given. In understanding the morphodynamics of intertidal flats, several processes can be distinguished such as hydrodynamic forces, sediment transport, and morphological changes. The bed properties are important in these processes. Intertidal flats experience complex hydrodynamic forcing, which is an important physical process that affects sediment transport and thus tidal flat morphology (de Swart and Zimmerman, 2009; Eisma, 1998; Friedrichs, 2011; Hir et al., 2000). fig. 2.6 after Zhu (2017) gives a good impression of the main components in understanding the morphodynamics on a tidal flat.

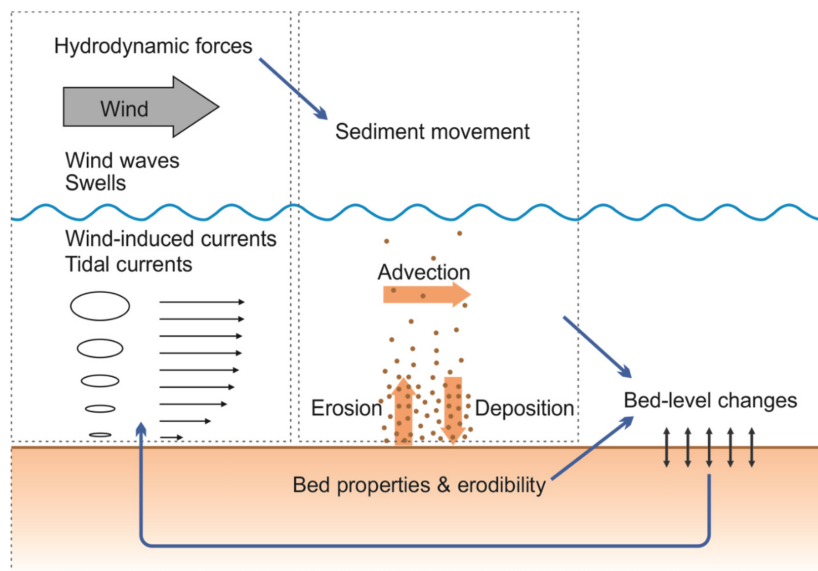


Figure 2.6 Schematization of sediment dynamic components. Hydrodynamic forces have an influence on the sediment movement (Zhu, 2017).

The movement of mud in an estuary depends on the hydrodynamic forcing caused by currents, waves and pressure gradients, and on gravitational forces on a sloping bed (Whitehouse et al., 2000).

When attempting to predict the movement of cohesive sediment, it is necessary first to investigate the nature of the hydrodynamics and then relate the movement of water to the movement of the cohesive sediment (Whitehouse et al., 2000, p. 12).

The main hydrodynamic variable that controls the erosion, suspension, and deposition of muds is the bed shear-stress τ , which is a frictional force exerted by the flow per unit area of the bed (Soulsby and Clarke, 2005).

Methods exist for calculating the bed shear-stress produced by currents and waves for muddy sediment. They are similar to the methods for coarse sediment only for muds it is typically assumed that the flow is hydrodynamically smooth in comparison to rough for sand and gravel (Whitehouse et al., 2000, p. 40). Before introducing the methods to calculate the bed shear stress, knowledge of boundary layer theory is presented.

2.2.1 Boundary layer theory

The following section describes the theory and assumptions behind the boundary layer (after Oertel (2003) and Elger et al. (2014)).

Consider a fluid flowing over a surface (fig. 2.7). Because of friction, the velocity of the fluid at the surface has the same velocity as the surface (no-slip condition) and must be zero. The region adjacent to the surface over which the velocity of the fluid changes from the free-stream velocity to zero at the surface is called the boundary layer. The thickness, δ , is defined as the distance at which the velocity is 99% of the free-stream velocity (in fig. 2.7 the region up to the edge of the outer layer). This layer exists because of the viscosity, μ , of the fluid, which is a property characterizing the resistance to flow. It can

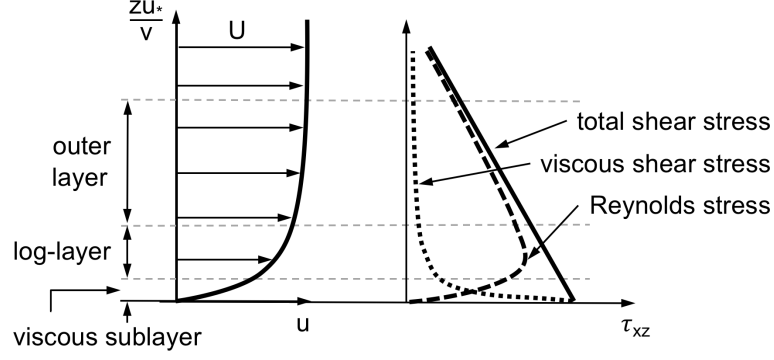


Figure 2.7 Velocity distribution close to the wall (left) and shear stress distribution (right) (after KANPUR (2018))

be defined as the ratio of shear stress, τ , to shear strain, du/dz . Hence, shear stress can be defined by eq. (2.1) (valid for Newtonian fluids).

$$\tau = \mu \frac{du}{dz} \quad (2.1)$$

A distinction can be made between a laminar boundary layer, turbulent boundary layer and a transition from laminar to turbulent. In a laminar boundary layer, the flow is smooth and steady whereas in a turbulent boundary layer intense cross-stream mixing and turbulent eddies are present. The mechanisms for the development of a boundary layer from laminar to turbulent will not be discussed here. Furthermore, only a fully developed turbulent boundary-layer will be considered.

In turbulent flow, small fluid masses are swept back and forth transverse to the main flow direction. Slowly flowing fluid mass that ends up in a faster flowing fluid mass slows down the faster flowing fluid mass and vice versa. This mechanism causes turbulent flow and consequently momentum exchange. The instantaneous velocity at a given point fluctuates with time because of the mixing and can be described by a mean part, \bar{u} , plus a fluctuating part, u' .

The fluctuating part can be described using the Prandtl mixing-length theory, which states that $u' = l d\bar{u}/dz$. Where the mixing length, l , is the path on which the fluid mass loses its individuality by turbulent mixing with the surrounding liquid.

The velocity fluctuations cause apparent shear stress, e.g., the turbulent shear stress or Reynolds stress (eq. (2.2)).

$$\tau' = -\overline{u'w'} \quad (2.2)$$

Using Prandtl mixing length theory the turbulent shear stress in eq. (2.2) can be described as eq. (2.3).

$$\tau' = -\overline{u'w'} = \rho l^2 \left(\frac{d\bar{u}}{dz} \right)^2 \quad (2.3)$$

Considering the flow over a surface, the mixing length must tend to zero closer to the surface. This implies that $d\bar{u}/dz$ becomes large close to the surface and small further away. The no-slip condition holds at the surface which forms a thin friction layer called the viscous sublayer.

For a smooth surface and constant shear stress, the total shear stress inside the turbulent boundary layer can be described by the mean value of the friction stresses and the apparent stresses of the turbulence (eq. (2.19)).

$$\begin{aligned} \bar{\tau} = \tau_w &= \mu \frac{d\bar{u}}{dz} - \overline{\rho u'w'} \\ &= \mu \frac{d\bar{u}}{dz} + \rho l^2 \left(\frac{d\bar{u}}{dz} \right)^2 \end{aligned} \quad (2.4)$$

The turbulent boundary layer has three zones of flow; the viscous sublayer, logarithmic region, and the velocity defect region. Only the first two regions will be considered. The viscous sublayer is the region immediately adjacent to the surface where the flow is essentially laminar because of the presence

of the wall that dampens the cross-stream mixing and turbulent fluctuations. The first part of eq. (2.19) is valid for this layer. The layer above the viscous sublayer is the logarithmic region, for which the second part of eq. (2.19) is valid. Between the viscous sublayer and the logarithmic region, a buffer zone exists. The region made up of the viscous sublayer, buffer layer and the logarithmic layer is called the law of the wall.

Introducing the shear stress velocity $u_* = \sqrt{\tau_w/\rho}$, the kinematic viscosity, $\nu = \mu/\rho$, and eq. (2.19) the velocity distribution can be deduced for both regions.

Viscous sublayer

Within the viscous sublayer the shear stress is constant and equal to the shear stress at the surface, τ_w . The velocity distribution in this layer can be described by eq. (2.5) for $zu_*/\nu \leq 1$.

$$\frac{\bar{u}}{u_*} = \frac{zu_*}{\nu} \quad (2.5)$$

From experiments with smooth surfaces, the viscous sublayer ranges for values of $zu_*/\nu \leq 5$.

In case of rough surfaces, the thickness of the viscous sublayer is in the order of magnitude of the roughness height, z_0 .

Logarithmic region

Above the viscous sublayer in the log-layer (fig. 2.7), it is assumed that the shear stress is uniform and approximately equal to the shear stress at the surface, τ_w . Prandtl made the important assumption that the mixing length is proportional to the distance from the surface, $l = \kappa z$. Substituting the mixing length, l , into the second part of eq. (2.19) and using the assumption of uniform stress, yields eq. (2.6) for the stress distribution in this layer.

$$u_*^2 = \kappa^2 z^2 \left(\frac{d\bar{u}}{dz} \right)^2 \quad (2.6)$$

From which the velocity distribution can be deduced after taking the square root and integration. Hence, the velocity distribution in this region is logarithmic and according eq. (2.7).

$$\frac{\bar{u}}{u_*} = \frac{1}{\kappa} \ln z + C \quad (2.7)$$

For smooth surfaces, the velocity distribution is according to eq. (2.8).

$$\frac{\bar{u}}{u_*} = \frac{1}{\kappa} \ln \frac{zu_*}{\nu} \quad (2.8)$$

For rough surfaces, the velocity distribution is according to eq. (2.9).

$$\frac{\bar{u}}{u_*} = \frac{1}{\kappa} \ln \frac{z}{z_0} \quad (2.9)$$

The logarithmic velocity distribution is valid for values of zu_*/ν ranging from approximately 30 to 500. This is because the mixing length cannot continuously increase towards the edge of the boundary layer.

Integration of eq. (2.7) over the vertical yields the depth averaged velocity U (Whitehouse et al., 2000).

$$U = \frac{u_*}{\kappa} \left[\ln \left(\frac{h}{z_0} \right) - 1 \right] \quad (2.10)$$

Buffer layer

Between the viscous sublayer and the logarithmic region, there is no expression for the velocity distribution. This region is called the buffer zone. In practice, the velocity profile in the viscous sublayer and the logarithmic zone are extrapolated to $zu_*/\nu = 11.84$.

The previously described regions indicated by zu_*/ν , are visualized in fig. 2.8.

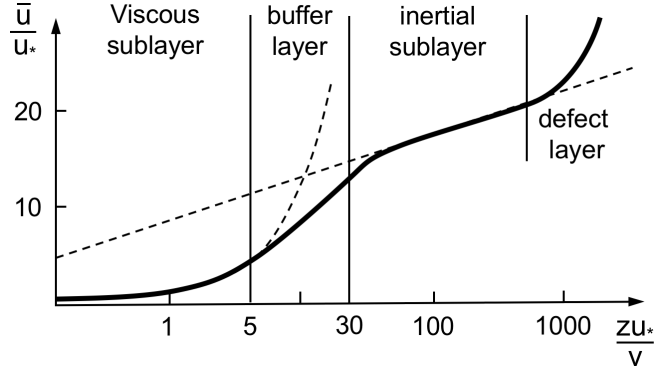


Figure 2.8 Velocity distribution close to the wall as a function of zu_*/ν

2.2.2 Log Profile (LP)

This method is based on the assumption of the law of the wall as described in § 2.2.1. If the flow is assumed to be neutrally stratified, horizontally homogeneous and stationary, a logarithmic profile is observed within the constant-stress layer where stress within the water column only varies slightly from bottom stress, t_w (Kim et al., 2000).

The logarithmic profile method relies on theoretical and empirical observations that shear in the bottom boundary layer is determined by a characteristic shear velocity u_* and height above the bottom z (see eq. (2.6) and fig. 2.7).

Application of the LP method requires measurements of *mean velocity* at several elevations in the log layer (at least two). u_* and z_0 can be estimated from least-squares fit, where \bar{u} is the dependent variable, $\ln z$ the independent variable, u_*/κ the slope and $-(u_*/\kappa \ln z_0)$ the intercept (Sherwood et al., 2006). The roughness length, z_0 , is defined as the intercept of the logarithmic velocity profile distribution. Meaning the depth at which the mean velocity is zero. According to (Andersen et al., 2007), the measurements should be carried out in the wave boundary layer.

2.2.3 Reynolds Stress (RS)

The Reynold Stress method, also known as "eddy correlation" method, relies on direct estimates of the horizontal components of turbulent shear stresses τ_{zx} and τ_{zy} associated with time-averaged correlation in turbulent velocity fluctuations. Furthermore, a logarithmic profile is assumed (Kim et al., 2000).

$$\begin{aligned}\tau_{zx} &= -\rho \overline{u'w'} \\ \tau_{zy} &= -\rho \overline{v'w'}\end{aligned}\quad (2.11)$$

Estimates of Reynold stresses based on measurements are very sensitive to small changes in the orientation of the current meter, and can also be biased by gentle slopes and weak reflected waves (Grant and Madsen, 1986; Trowbridge, 1998).

Trowbridge (1998) proposed a method for reducing wave-induced bias in Reynolds stress estimates by using two measurements of velocity at separate locations. The estimate of $\overline{u'w'}$ then becomes:

$$\overline{u'w'} \approx \frac{1}{2} \text{cov}(\Delta u, \Delta w) = \frac{1}{2} \overline{\Delta u' \Delta w'} + \frac{1}{2} \overline{\Delta \tilde{u} \Delta \tilde{w}} \quad (2.12)$$

Where u and w are measured velocity components in the sensor coordinate system and Δ the difference between the quantities measured at the two locations.

To relate u_* to Reynolds stresses it is assumed that the measurements are in the constant-stress region (Sherwood et al., 2006). In a log layer $\overline{u'w'}$ are related to u_* according (Kim et al., 2000; Tennekes and Lumley, 1972).

$$\frac{-\overline{u'w'}}{u_*^2} = 1 - \frac{1}{\kappa u_* z / \nu} = 1 - \frac{1}{R} \quad (2.13)$$

For fully turbulent flow with large Reynolds number, $R \gg 1$, u_*^2 becomes $-\overline{u'w'}$.

The Reynold Stress method is not dependent on z (Kim et al., 2000). Application of the Reynold Stress method requires high-frequency, three-axis velocity measurements at two locations (Sherwood et al., 2006). This method is particularly sensitive to sensor misalignment and can give errors up to 156 percent per degree of misalignment in wave-dominated conditions (Soulsby and Humphrey, 1989).

2.2.4 Turbulent Kinetic Energy (TKE)

The absolute intensity of velocity fluctuations (variances) can be used to infer bed stress through turbulent kinetic energy (TKE)

The TKE can be described by

$$E = \frac{1}{2}(\overline{u'^2} + \overline{v'^2} + \overline{w'^2}) \quad (2.14)$$

Soulsby and Dyer (1981) found that the average ratio of shear stress to TKE is constant

$$|\tau| = C_1 E \quad (2.15)$$

Where the proportionality constant $C_1 \sim 0.19$ according Stapleton and Huntley (1995).

Application of the TKE method requires high-frequency, three-axis velocity measurements from which the turbulent fluctuation can be deducted.

2.2.5 Vertical Turbulent Kinetic Energy (TKEw)

The vertical turbulent kinetic energy method is similar to the TKE method but uses the vertical velocities alone. Hence, when a linear relation is assumed, the bottom stress related to a variance component reads $|\tau| = C_2 \overline{w'^2}$. Where the proportionality constant $C_2 \sim 0.9$ according Kim et al. (2000).

The RS method is the most fundamental method since it directly estimates the momentum flux towards the seabed.

On the applicability of the methods

The LP is not a fundamental method because they depend on semi-empirical models that might not be valid for a particular set of measurements. It relies on the law of the wall which is an empirical model known to be valid in the constant-stress region of an unstratified boundary layer. It assumes a logarithmic velocity profile over the depth. Causes of non-logarithmic profiles on intertidal flats are described by (Collins et al., 1998). They are rotary tidal currents, wind effects, wave action other short period oscillations and topographically-induced secondary flow. For the LP method to minimize the effect of waves, a very calm period should be chosen for estimating the current-induced bed shear-stress (Andersen et al., 2007).

The methods described have been applied in several field experiments, but generally only in situations where currents dominate and water depths are larger than one meter (Andersen et al., 2007). When the wave-orbital velocities are, e.g., five times larger than the mean current velocities, application of the TKE and RS methods becomes difficult. The orbital velocities and turbulence have to be filtered from the TKE which relies on accurate determinations of the inertial subrange (Andersen et al., 2007). TKEw method is insensitive to waves, but for this method, measurements should not be too close to the bed (Andersen et al., 2007).

The RS method should be valid under waves and requires the linear wave theory assumption of $\overline{u'w'} = 0$ and $\overline{v'w'} = 0$. The latter may not be the case in very shallow water (Andersen et al., 2007).

2.3 Data analysis

The data analysis part consists of calculating the bed shear stress and corresponding bed roughness parameters. Four methods were applied to calculate the bed shear stress. These methods can be divided into first momentum methods which are based on mean velocities and second momentum methods which are based on fluctuating velocities. The first momentum method uses the assumption of a logarithmic velocity profile to obtain values for the friction velocity and the roughness height (z_0). In § 2.3.1 this method is explained. In § 2.3.2 the second momentum methods are elaborated.

2.3.1 Bed shear stress using first momentum methods

The first momentum method used in this thesis is the logarithmic profile method (LP). The velocity profile follows a logarithmic profile according to the law of the wall.

This velocity can be described by:

$$u(z) = \frac{u_*}{\kappa} \ln \left(\frac{z}{z_0} \right) \quad (2.16)$$

The ADCP instruments measure velocities in all three directions with a frequency of 1 Hz, meaning that each second velocity measurements are performed. Since the ADCP measures at multiple levels above the bed, a velocity profile can be deduced. One velocity profile is obtained for each minute by taking the average of all the velocity profiles over a duration of 60 seconds. At each height above the bed, the absolute velocity is calculated using eq. (2.17).

$$U = \sqrt{u^2 + v^2} \quad (2.17)$$

An example of measured profiles converted to a single velocity profile can be seen in fig. 2.9. Besides averaging the magnitude of the horizontal velocity components, the acoustic parameters are averaged at each height. Each velocity point of the profile is considered separately, and the acoustic parameters for this point are verified. The data point is assumed to be of good quality when the correlation $\geq 70\%$ and the amplitude ≥ 100 counts. After the quality check at least 4 points in the profile should remain and these points should be below the water surface.

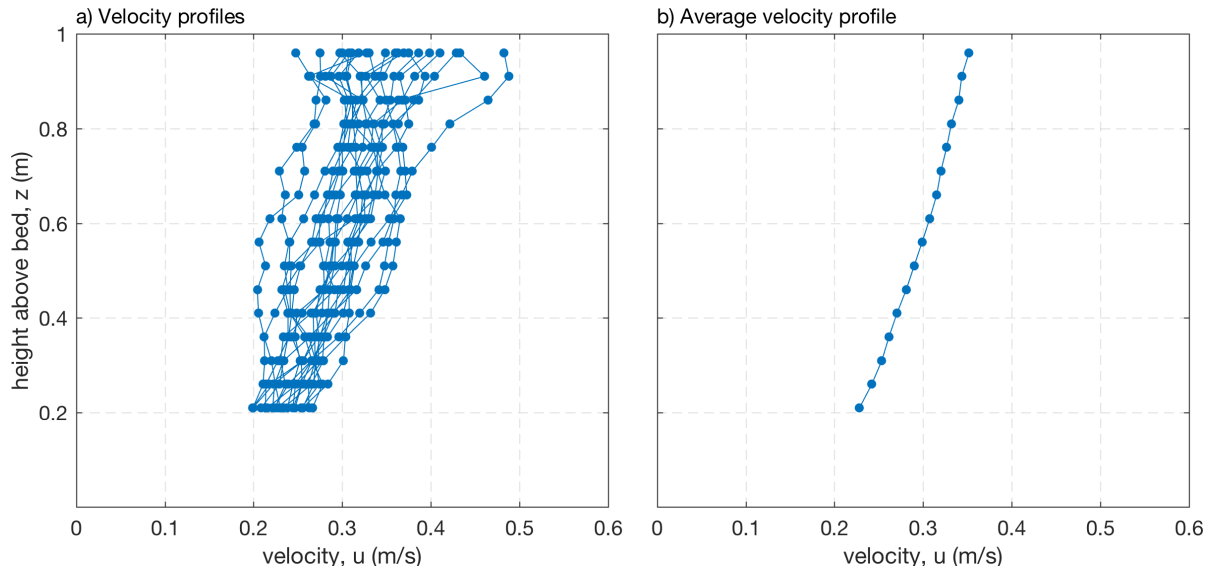


Figure 2.9 Averaging of a group of velocity profiles in order to apply the logarithmic profile method.

To obtain values for u_* and z_0 in eq. (2.16), the current speed u is linearly regressed against the natural logarithm $\ln z$ using the least-squares method. This yields two coefficients representing the best linear fit. The intercept at which the vertical axis is crossed is denoted as b , and the slope of the linear fit is denoted as a . u_* and z_0 can be expressed in terms of the intercept b and slope a as in eq. (2.18).

$$\begin{aligned} u_* &= \kappa a \\ z_0 &= e^{-\frac{b}{a}} \end{aligned} \quad (2.18)$$

To get to the bed shear τ , the expression in eq. (2.19) is used.

$$\tau = \rho u_*^2 \quad (2.19)$$

2.3.2 Bed shear stress using second momentum methods

The second momentum methods rely on the velocity fluctuations. The three methods applied are the turbulent kinetic energy (TKE), modified turbulent kinetic energy (TKEw) and Reynolds stress (RS) method. The formulae are described in table 2.2. Flow subjected to bed friction results in a turbulent boundary layer which can extend to the water surface (Whitehouse et al., 2000). The velocity signal in this layer can be described as a mean velocity plus a fluctuating velocity.

$$u = \bar{u} + u' \quad v = \bar{v} + v' \quad w = \bar{w} + w' \quad (2.20)$$

Hence, the high frequent velocity signals obtained from the ADV instruments can be used to obtain the fluctuating velocities.

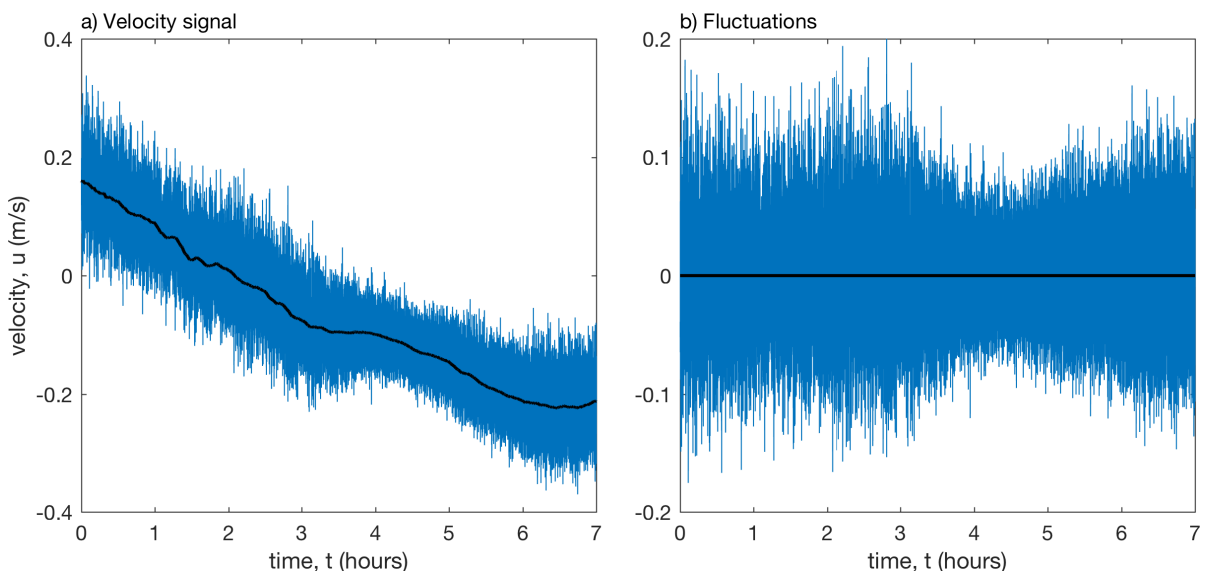


Figure 2.10 Measured velocity signal during an ebb tidal phase, including the moving mean by taking a window of 10 minutes.

In fig. 2.10 an example of a velocity signal is shown. In fig. 2.10a the velocity signal is based on a non-stationary flow and in fig. 2.10b the mean flow velocity is subtracted to keep only the fluctuations.

In this study, the velocity signal is mainly non-stationary, and thus a moving mean needs to be applied to find the mean velocities in eq. (2.20). This moving mean can be calculated by taking the mean value of a quantity for N data points with $N/2$ points before and $N/2$ points after the point of interest. This window of N points is moving forward in time to the last point. However, no moving average is applied because it is assumed that the velocity remains constant for one minute. Thus, the mean velocity is calculated by taking the mean velocity over N points and assuming that this value is the same for all N points. For the next N points, the same analogy is followed. The mean is calculated over 480 data points, for a device measuring with a frequency of 8 Hz this means 10 min. Moments where the velocity is not measured (i.e., the instrument is out of the water) are not taken into account for the calculation of the mean.

Bed shear stress

After defining the turbulent fluctuations at each measured moment in time, the three second momentum methods can be applied to obtain the bed shear stress. The applied formulae are summarized in table 2.2. The bed shear stress is calculated for 60 seconds.

2.3.3 Bed roughness parameters

This roughness can be expressed with the bed roughness length z_0 , Nikuradse roughness k_s , Chezy C or Manning n .

Table 2.2 Second moment methods (TKE, TKEw, RS) for estimating current-induced bed shear-stress

Method	Formulae	Coefficients
TKE Turbulent Kinetic Energy	$\tau = C \cdot \rho_w \cdot \frac{\overline{u'^2} + \overline{v'^2} + \overline{w'^2}}{2}$	$C = 0.19$ (Stapleton and Huntley, 1995)
TKEw Vertical Turbulent Kinetic Energy	$\tau = C \cdot \rho_w \cdot \overline{w'^2}$	$C = 0.9$ (Kim et al., 2000)
RS Reynolds Stress	$\tau = \rho_w \cdot \sqrt{\overline{u'w'^2} + \overline{v'w'^2}}$	

For hydrodynamically rough ($u_* k_s / \nu \geq 70$) or transitional ($5 < u_* k_s / \nu < 70$) beds the roughness length is expressed in eq. (2.21a) and for hydrodynamically smooth ($u_* k_s / \nu \leq 5$) in eq. (2.21b) (Whitehouse et al., 2000, p. 43-45).

$$z_0 = \frac{k_s}{30} \left[1 - \exp\left(\frac{-u_* k_s}{27\nu}\right) \right] + \frac{\nu}{9u_*} \quad (2.21a)$$

$$z_0 = \frac{\nu}{9u_*} \quad (2.21b)$$

Where k_s is the Nikuradse roughness The kinematic viscosity ν of water decreases with temperature and increases with salinity. (Soulsby, 1997, p. 25) When fresh water is added, the salinity changes and thus the kinematic viscosity. Furthermore, it can cause density currents.

Bed roughness values can be calculated by assuming a logarithmic profile. From eq. (2.19) one can derive the friction velocity which can be implemented in eq. (2.16). The only thing remaining is the velocity u and the depth z . This is known as the ADV measures 3D velocities at a fixed distance from the bed. The expression for the bed roughness then becomes after rewriting eq. (2.16).

$$z_0 = z \cdot \exp\left(\frac{-\kappa u}{u_*}\right) \quad (2.22)$$

For the four bed, shear-stress methods z_0 can be derived. Other roughness parameters which can be calculated from this are in table 2.3.

Table 2.3 Roughness parameters

Roughness parameter	Formula
Nikuradse roughness	$k_s = 30z_0$
White-Colebrook	$C = 18 \log_{10} \frac{12h}{k_s}$
Manning	$n = \frac{\sqrt[6]{h}}{C}$

2.3.4 Tidal reversal

In fig. 2.11 five days of the measured waterdepth and velocity signal are shown. For calculating tidal phase averaged values, it is necessary to find the moment when the tide reverses. To find these moments, the velocity signal is analyzed. When the tidal flow changes direction, the tide goes from flood to ebb or vice versa. Since the velocity signal is not continuous, the signal is made continuous by linear interpolation. Before interpolating, the fluctuations in the velocity signal are reduced by applying a moving mean with a window of 10 minutes. After the interpolation, the resulting velocity signal is smoothed once again with the same window.

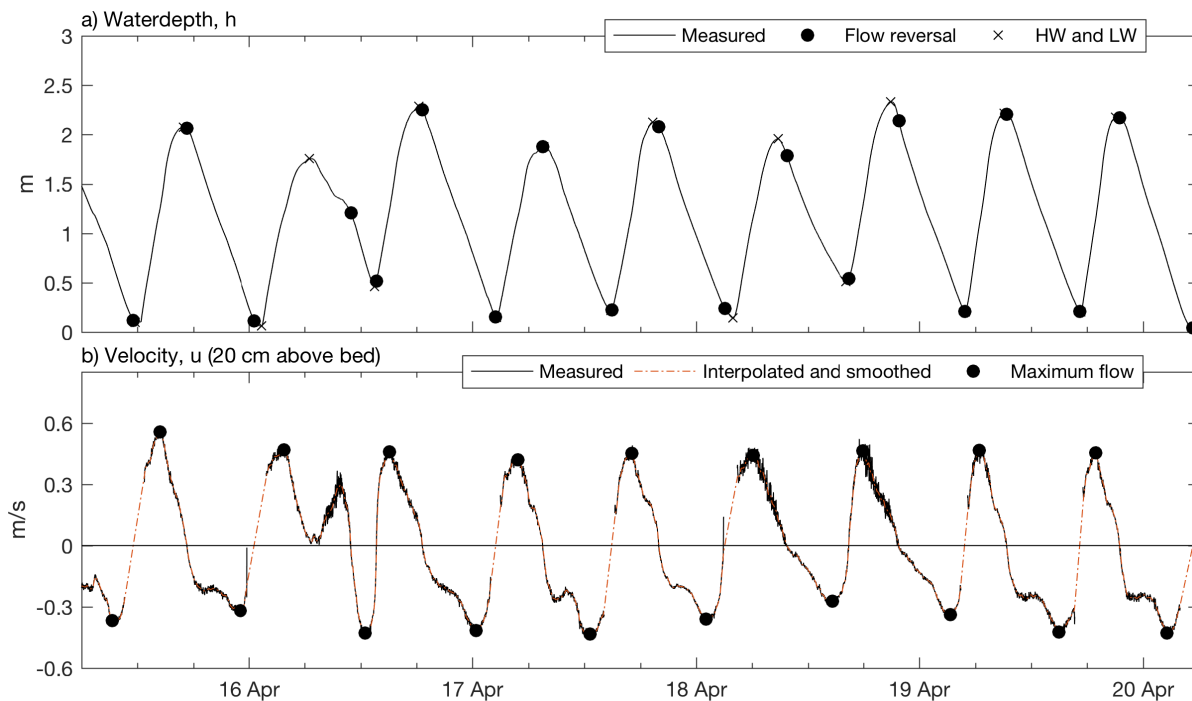


Figure 2.11 (A) Waterdepth and (B) velocity at 20 cm above measured at offshore frame for a period of five days, showing 9 tidal cycles

The moments of turning of the tide can now be determined by searching for moments where the tidal flow velocity changes direction.

Extreme tidal flow velocities are determined by finding the extreme flow velocity between two turnings of the tide. This analysis is performed on the interpolated velocity signal, and the outcome is indicated with dots in fig. 2.11b.

A similar approach can be followed to find the extremes in the water depth signal. By looking at the extreme water depth between two extreme flow velocities the moments of LW and HW can be determined. The outcome of this analysis is shown in fig. 2.11a indicated by crosses.

It can be observed that the turning of the tide not always coincides with extreme water depths. For example between 16th Apr and 17th Apr. The previously described analysis is performed on the full measuring period and shows similar results as in fig. 2.11.

2.3.5 Tidal analysis

Besides the determination of the turning of the tide, the major tidal components are determined using a Matlab script provided by Codiga (2011). This analysis is performed on the astronomical prediction at Harlingen obtained from Rijkswaterstaat (2016). The result of this analysis is shown in table 2.4.

Table 2.4 Major tidal components. Obtained from tidal analysis on the astronomical prediction from Rijkswaterstaat (2016)

Component	Amplitude (m)	Period (hr)	Phase (deg)
M2	0.830	12.42	331.9
S2	0.214	12.0	38.0
N2	0.156	12.66	296.0
L2	0.129	12.19	341.1
M4	0.114	6.21	193.1
MU2	0.111	12.87	58.6
O1	0.093	25.82	258.1

2.3.6 Statistical analysis

Two types of statistical analysis were performed on the dataset. First of all, averaging per tidal phase (§ 2.3.4). Averaging is done using an arithmetic mean or geometric mean. The latter is determined by taking the average of the natural logarithm of the quantity and taking the natural exponent of the outcome. The geometric mean is typically performed on quantities varying in order of magnitudes such as the roughness length, z_0 .

The averages of a quantity per tidal phase are used to perform an auto-correlation and partial auto-correlation analysis.

Statistical models such as an autoregressive–moving-average model (ARMA), are used to find relations between multiple quantities by a linear fit using least square method.

2.4 Modeling

Numerical modeling is performed to gain insight into the formation of a two-layered fluid system (fluid mud) using a 1DV point model. This model is more thoroughly described in Winterwerp and van Kesteren (2004). A 1DV instead of a 3D model is used to eliminate advection.

This model is developed on the basis of Delft3D-FLOW (software developed by Deltares to simulate water movement and transport of matter in 3D). In this model, a 1DV-equation for horizontal momentum is used. In the 1DV point model horizontal advection terms are omitted; furthermore, a flat and horizontal bed is assumed (Winterwerp and van Kesteren, 2004).

2.4.1 Model description

Using the numerical model, two types of simulations will be conducted. One type where stationary boundary conditions are imposed and one with transient boundary conditions. Simulations with stationary conditions are performed to find out for which conditions a fluid mud layer can be formed. Simulations with pre-scribed time-series of boundary conditions are performed to find out if and at which timescales a fluid mud layer can be formed. In table 2.5 the model parameters for both types of simulations are given.

Table 2.5 Parameter settings for simulations with stationary and transient boundary conditions.

Parameter	Symbol	Value	Remarks
Water depth, m	h	variable	Equidistant varying from 0.2 to 2.8 in steps of 0.1 m
Depth-averaged flow velocity	U	variable	Equidistant varying from 0.05 to 0.7 in steps of 0.05 m/s
Bed roughness	z_0	1 mm	
Water density	ρ_w	1020 kg/m ³	
Sediment density	ρ_w	2650 kg/m ³	
Initial sediment concentration	C_0	variable	
Settling velocity	W_s	9×10^{-4} m/s	
Hindered settling		yes	
Gelling concentration	c_{gel}	80 g/L	
Water bed exchange		no	
Prandtl-Schmidt number	σ_T	0.7	
Number of layers		200	Equidistant
Time step	Δt	variable	Based on criterium to accomodate for advective effects properly: $\Delta t < \Delta z/w_s$
Relaxation time	T_{rel}	$2\Delta t$	

The settling velocity is chosen at 9×10^{-4} m/s and is based on Stokes' formula for a stationary settling particle. The particle diameter is assumed to be 30 μm .

2.4.2 Simulations with stationary boundary conditions

A matrix of hydrodynamic conditions is used where each combination is investigated for the formation of fluid mud. For each combination, homogeneous initial concentrations are imposed and simulated. The initial concentration is gradually increased until an initial concentration is found at which the concentration profile collapses.

The homogeneous initial concentrations C_0 are varying non-equidistant from 0.002 to 100 g/l. The following list gives the concentrations which are applied.

- From 0.002 to 0.01 in steps of 0.002 g/l.
- From 0.01 to 0.1 in steps of 0.005 g/l.
- From 0.1 to 1.0 in steps of 0.05 g/l.
- From 1 to 10 in steps of 0.5 g/l.

- From 10 to 100 in steps of 5 g/l.

In determining whether the concentration profile collapses, the Rouse number of two consecutive simulations are compared. If the ratio between the two Rouse numbers is larger than 1.35 a collapse of the concentration profile is assumed.

The simulations carried out under stationary conditions are simulated for a total simulation period of 240 minutes ((Winterwerp, 2001) discusses the timescales at which fluid mud is formed). All the simulations are carried out without wind and wave forcing.

2.4.3 Simulations with transient boundary conditions

Simulations with transient boundary conditions will be executed where the total simulation time is one tidal phase. A time-series of water depth and depth-averaged velocity will describe the boundary conditions for these simulations. These time-series will be obtained from the dataset, and a tidal cycle with mild wind conditions will be chosen to minimize the influence on the depth-averaged flow velocity and the water depth.

2.4.4 Roughness determination from model results

From the two types of simulations conducted with the 1DV point model, the roughness length z_0 will be computed using the LP method. For the simulations with stationary conditions, one combination of water depth and velocity will be picked out. The roughness will then be determined for each initial concentration and based on the velocity profile at the end of the simulation period, the roughness is calculated. For the simulations with transient conditions, the roughness is determined for each timestep during the tidal cycle, so for each velocity profile obtained from the model.

3

Results

The results of this thesis are divided into a part where the data from observations is analyzed and a part where outcomes of the data analysis are investigated with a numerical model described in § 2.4.

3.1 Data analysis

3.1.1 Description of observations

The offshore frame measured for 39 days and recorded 78 tides (figs. 3.1 and 3.2). Time series of water depth, velocity, wind and wave height (H_{m0}) are in fig. 3.1. The water depth and velocities are averaged per minute and obtained from the ADV measuring in continuous mode. Wind velocities and directions are obtained per 10 minutes. A spring-neap tidal cycle can be observed (fig. 3.1a) with a tidal range varying between 1.25 m and 2.44 m. Maximum tidal flow velocities range from 38 to 56 cm/s during flood and 27 to 69 m/s during ebb. Although the maximum flow velocities during ebb are larger, on average the flood velocities are larger than ebb velocities. Furthermore, the flood duration is generally shorter than ebb.

In these figures periods of calm and strong winds can be distinguished. High wind velocities coincide with high waves and an erratic velocity signal. For these periods the friction velocity and bed shear stress increase as well. When waves are high, the suspended sediment concentration at 6 and 11 cm above the bed increases which could indicate stirring of sediment by the waves (fig. 3.2f). A relation between suspended sediment concentration and wind direction is not directly clear from the figures.

Because of the relatively shallow area, the wind can have a strong influence on the tidal flow. This can be seen in fig. 3.1b, where the tidal flow is counteracted during ebb for T4 and T29. For these tides, the velocity stays or becomes positive during the ebb tidal phase. For T4 the wind comes from SW with a wind speed of more than 10 m/s, whereas for T29 the wind blows from the south with more or less the same wind speed.

Suspended sediment concentration for the observed period shows reasonably similar magnitudes (fig. 3.2f). For some consecutive days, the maximum suspended sediment concentration per tide keeps gradually increasing or decreasing per tide. This is mainly the case when the wind is blowing for several days with more or less the same wind speed and direction. For example, the period from 22nd Apr to 26th Apr where the wind primarily blows from NW with at least 5 m/s. A similar period can be found between 8th May and 14th May where the wind gradually rotates from east to northeast. Around 24th May the maximum suspended sediment concentration also increases but far less gradual. In this case, the wind is coming from the north.

It is clear from figs. 3.1 and 3.2 that the wind can have a significant influence on the tidal flow and suspended sediment concentration. The result of this will be further elaborated in § 3.1.4.

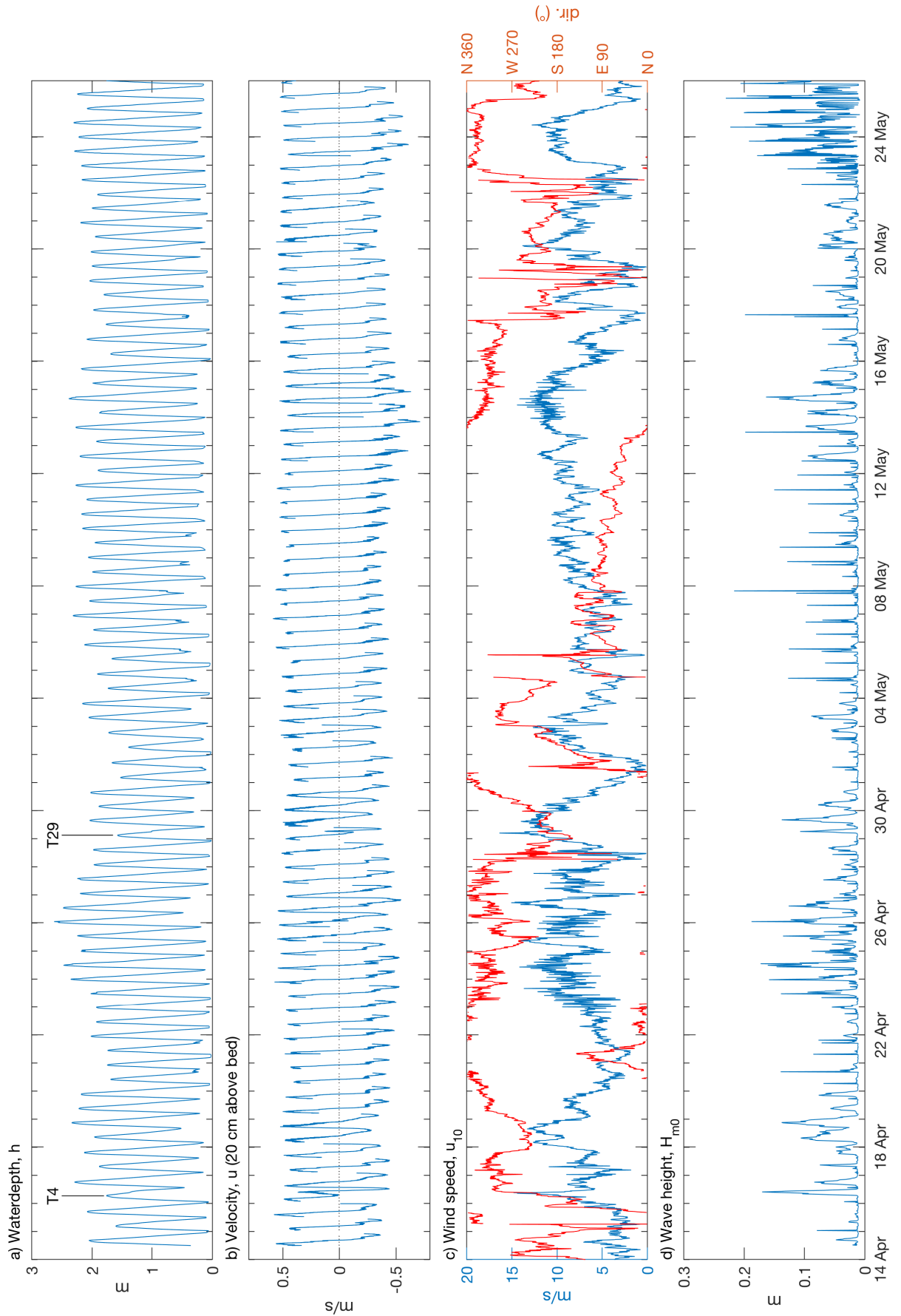


Figure 3.1 Time series of (a) waterdepth (b) velocity at 20 cm above the bed (c) wind speed and direction measured at Noorder Balgen station, (d) H_{m0} using zero-crossing method; over the full period of observational data.

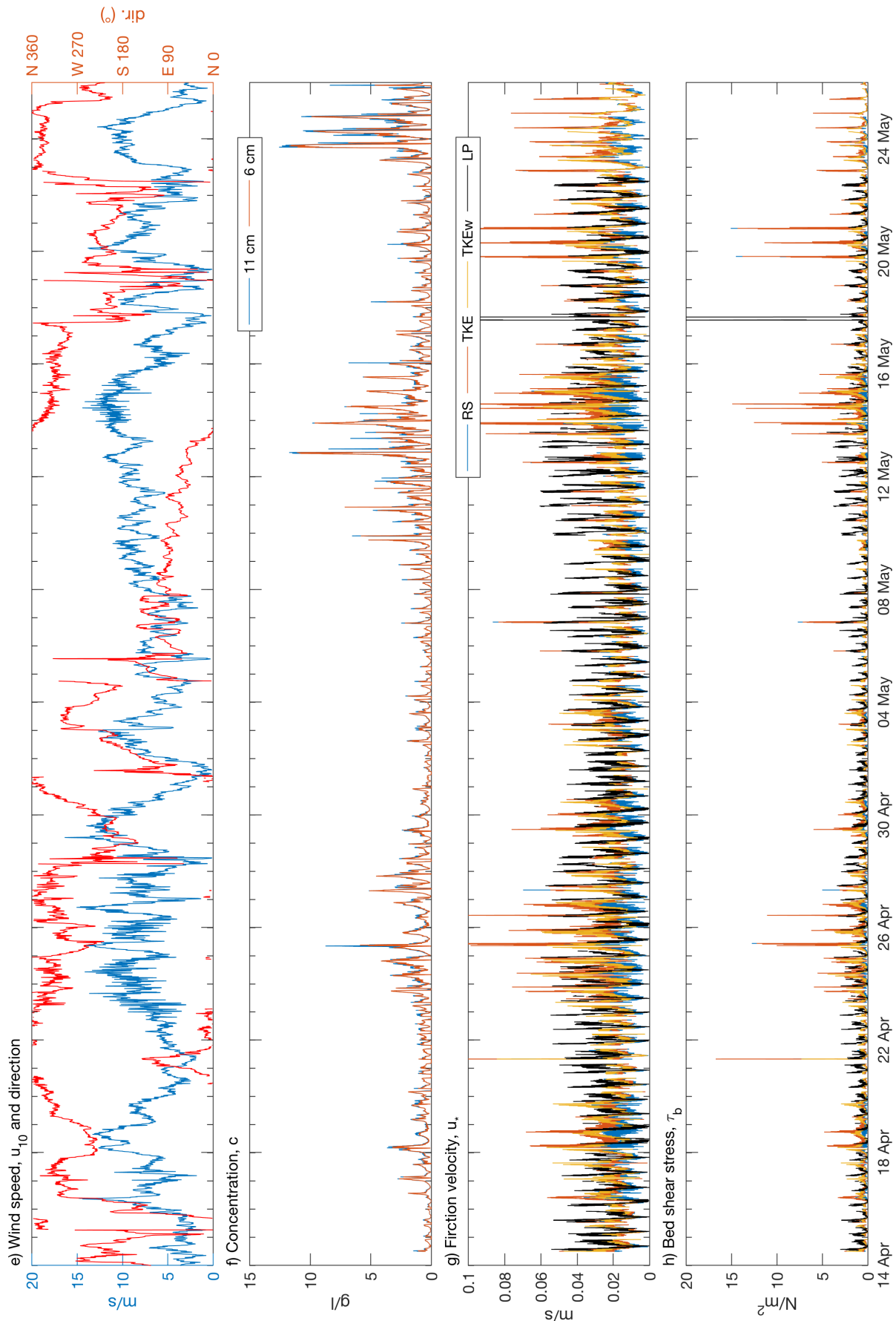


Figure 3.2 Time series of (e) wind speed and direction measured at Noorder Balgen station, (f) suspended sediment concentrations measured 6 and 11 cm above the bed (g) friction velocity u_* determined from the four bed shear stress methods and (h) bed shear stress τ_b over the full period of observational data

3.1.2 Bed shear stress calculations

From the observations described in § 3.1.1 the bed shear stress is calculated using methods described in § 2.3.1 and § 2.3.2.

Bed shear stress, friction velocity u_* and the roughness length z_0 are determined using the formulae described in § 2.3.3. The results of the bed shear stress are filtered such that the roughness is only calculated when the logarithmic profile gives a good fit, this is when the goodness of fit is larger than 95 % (fig. 3.2g and fig. 3.2h). The intra-tidal variation of bed shear stress and suspended sediment concentration is evaluated using a 4-day period from 2nd May till 5th May in response to wind and tides.

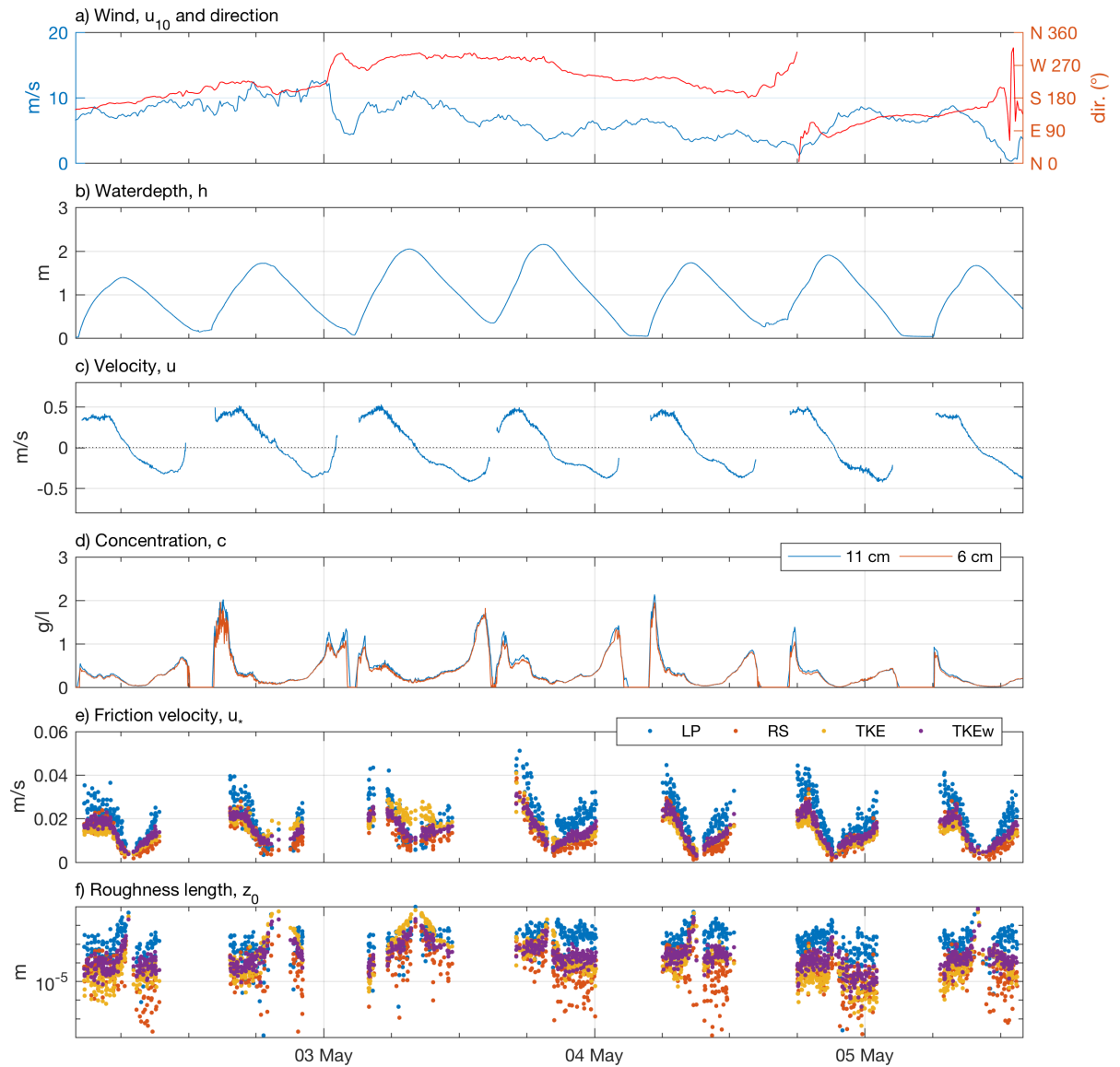


Figure 3.3 Time series of (a) wind speed and direction measured at Noorder Balgen station, (b) waterdepth at offshore frame (c) velocity measured at 20 cm above the bed (d) suspended sediment concentration (e) friction velocities derived from the four bed shear stress methods and (f) estimations of roughness length z_0

The measured concentrations between 6 and 11 cm above the bed increase with wind speed (fig. 3.3d). At the same time, the velocity signal at 20 cm above the bed becomes more erratic indicating more turbulent fluctuations. There is hardly any difference notable between the measured concentrations at 6 and 11 cm from the bed. During low water, the concentrations decrease to zero because the OBS is out of the water.

Table 3.1 Roughness length z_0 in meters averaged per tidal phase using an arithmetic mean. T1 to T7 represent the tides in fig. 3.3

		T1	T2	T3	T4	T5	T6	T7
LP	flood	2.9×10^{-3}	1.2×10^{-3}	5.3×10^{-3}	4.7×10^{-3}	5.6×10^{-3}	2.9×10^{-3}	7.2×10^{-3}
LP	ebb	6.9×10^{-4}	1.2×10^{-2}	4.7×10^{-3}	4.5×10^{-3}	5.5×10^{-3}	7.6×10^{-4}	1.6×10^{-2}
TKE	flood	3.2×10^{-4}	1.3×10^{-3}	7.5×10^{-3}	2.1×10^{-3}	1.8×10^{-3}	9.4×10^{-5}	7.2×10^{-4}
TKE	ebb	2.8×10^{-5}	4.5×10^{-3}	1.0×10^{-2}	4.0×10^{-4}	4.1×10^{-4}	2.5×10^{-5}	3.4×10^{-4}
TKEw	flood	4.2×10^{-4}	5.4×10^{-4}	1.7×10^{-3}	1.1×10^{-3}	1.4×10^{-3}	2.4×10^{-4}	1.2×10^{-3}
TKEw	ebb	9.6×10^{-5}	1.5×10^{-3}	2.4×10^{-3}	2.1×10^{-4}	3.2×10^{-4}	4.1×10^{-5}	3.5×10^{-4}
RS	flood	4.1×10^{-4}	1.5×10^{-4}	8.4×10^{-4}	8.5×10^{-4}	7.1×10^{-4}	1.2×10^{-4}	9.4×10^{-4}
RS	ebb	2.1×10^{-5}	1.8×10^{-4}	1.5×10^{-3}	7.4×10^{-5}	5.3×10^{-5}	1.9×10^{-5}	4.7×10^{-5}

Sediment concentration peaks coincide with flow velocity maxima, but there is a considerable variability in suspended sediment concentration between different tidal cycles.

Friction velocity and roughness length show variations over time during a tidal phase (fig. 3.3f). The roughness differs per method. In general, the roughness determined from second momentum methods give lower roughness compared to the logarithmic profile method. Overall the RS method gives lower roughness values followed by TKE and TKEw method.

3.1.3 Tide phase averaged roughness

The previous section (§ 3.1.2) elaborated on the variation of bed shear stress methods. Average roughness values are determined using an average per flood and ebb phase during a tidal cycle. Averaging is also performed for the wind speed, wind direction, roughness length and concentration per tidal phase for the full measuring period of 39 days (fig. 3.4).

During periods of low concentrations (between 1st May and 9th May for example) the roughness length is lower and more variable between consecutive tidal phases (fig. 3.3). When looking at the period between 24th Apr and 28th Apr, the concentration is higher, and the methods give higher roughness values. In this period the wind mainly blows from the NW around 10 m/s. A similar situation is present between 12nd May and 16th May where the concentration is even higher, but now the wind is mainly blowing between north and east. During low wind speed, the suspended sediment concentration and roughness are lower whereas, during high wind speed, the suspended sediment concentration and roughness is higher (fig. 3.3). It is not directly evident if the roughness is higher during flood or ebb.

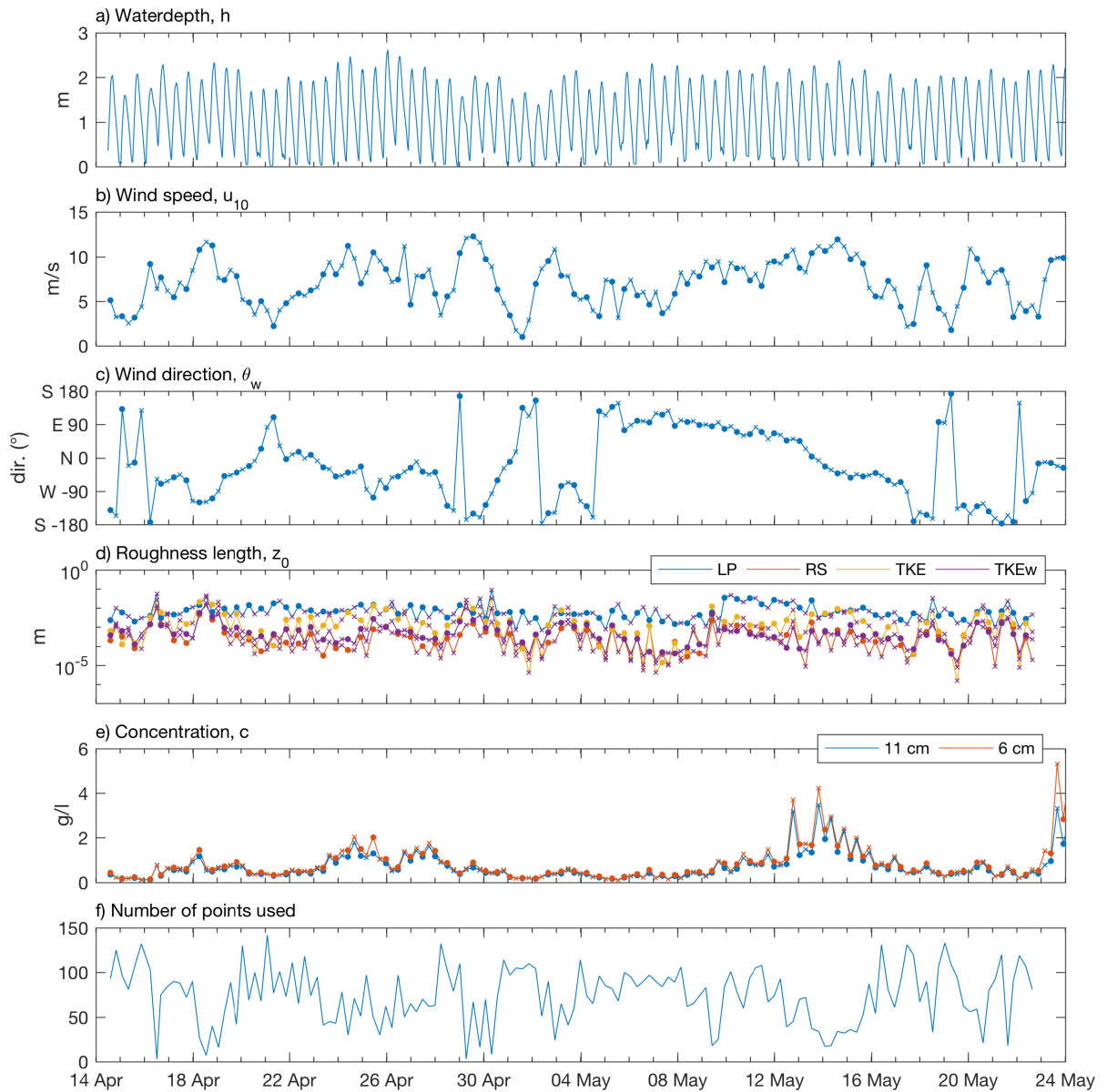


Figure 3.4 Time series of tidal phase averaged quantities (A) waterdepth (B) wind speed (C) wind direction (D) roughness length (E) concentration and (F) number of points used for averaging. Flood phases are marked with filled circles and ebb phases with a cross.

3.1.4 Statistical analysis

To investigate what mechanism causes the variation in roughness observed in the time series, an attempt is made in finding relationships using a statistical approach. In fig. 3.5 the tidal phase averaged wind speed is plotted together with the tidal phase averaged concentration. From this figure, it can be observed that the order of magnitude of the concentration follows the wind speed quite well except for tides around 30th Apr. Overall the peaks in concentration coincide with the peaks in wind speed. This indicates there is a relation between the wind speed and concentration of SPM measured at 6 cm above the bed.

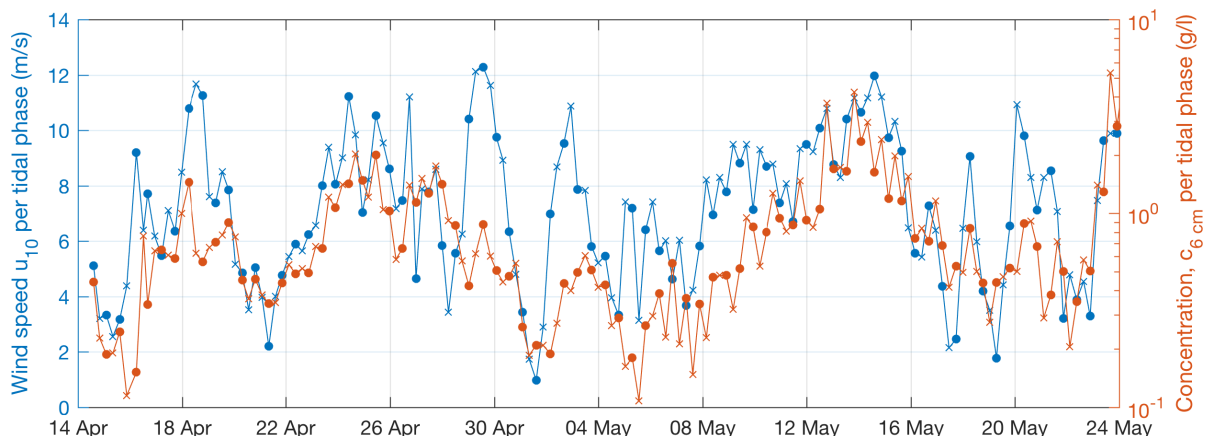


Figure 3.5 Time series of tidal phase averaged wind speed and concentration.

Wind speed is plotted against concentration at 6 cm above the bed (fig. 3.6). A distinction is made between ebb and flood tidal phases. A trend is visible where a higher wind speed indicates a higher suspended sediment concentration above the bed. This is the case for flood as well as ebb.

As an addition to the previously mentioned result, an auto-correlation and partial auto-correlation analysis is performed on the time series of SPM supplemented with wind information (appendix A). The result of this analysis (figs. A.1 to A.4) indicates that the concentration of SPM is an auto-regressive process of order two. This means that the concentration of SPM at time t can be modeled as a function of the concentration of SPM at time $t-1$ and $t-2$. This means there is a history effect in the concentration of SPM. Whether the concentration is increasing or decreasing depends on the wind speed (fig. 3.5). The local amount of SPM is not an instantaneous process but requires time to arrive or being carried away. With higher winds, the sediment concentration will increase, and with lower winds, it will decrease. The statistical model explains about two-thirds of the variation, and the auto-correlation of the residuals is reasonably well behaved. Meaning that the statistical model can explain the history effect mentioned before.

In fig. 3.7 tidal phase averaged roughness from the LP method is described as a function of the tidal phase averaged concentration of SPM on a double log scale. Although there is a spread, a trend is visible for the LP method. The spread is more pronounced for the methods based on turbulent fluctuations. In figs. A.3 and A.4 a statistical model is applied to the concentration of SPM and roughness based on the LP method. From the statistical model and the relation described in fig. 3.7 it can be concluded that the sediment becomes rougher with increasing concentration of SPM at 6 cm. So an increase in suspended sediment concentration indicates a higher roughness. This suggests that suspended sediment is not primarily governed by advection but also by local resuspension. This physically means that sediment is resuspended under high wind conditions and remains in the water column because it has difficulty resettling. Eventually resulting in a bed where fine sediments are brought into suspension arriving at a bed with rougher sediments.

For the difference in roughness between flood and ebb no consistent signal is visible (fig. 3.4).

A principal component analysis (PCA) is applied on the estimations of the roughness to reveal the correlation structure between the four methods. The results are described in figs. A.5 to A.8. The three turbulent kinetic energy methods are mutually very correlated (figs. A.5 and A.6) but differ from the logarithmic profile method. Therefore, the behavior of the three TKE methods is summarized in fig. A.6 and appears to depend on wind speed, wind speed at the previous tidal phase, wind direction

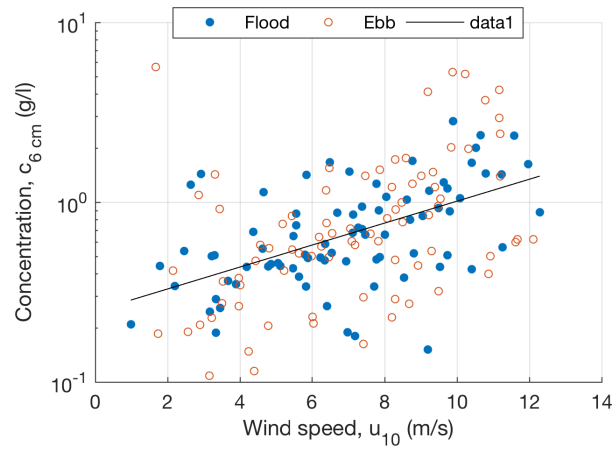


Figure 3.6 Correlation between wind speed and concentration. The solid line drawn, represents a trendline using the least squares method.

and whether the tidal phase is ebb or flood. However, there is no dependency on sediment concentration which is in contrast with the statistical model for z_0 based on the logarithmic profile mentioned earlier.

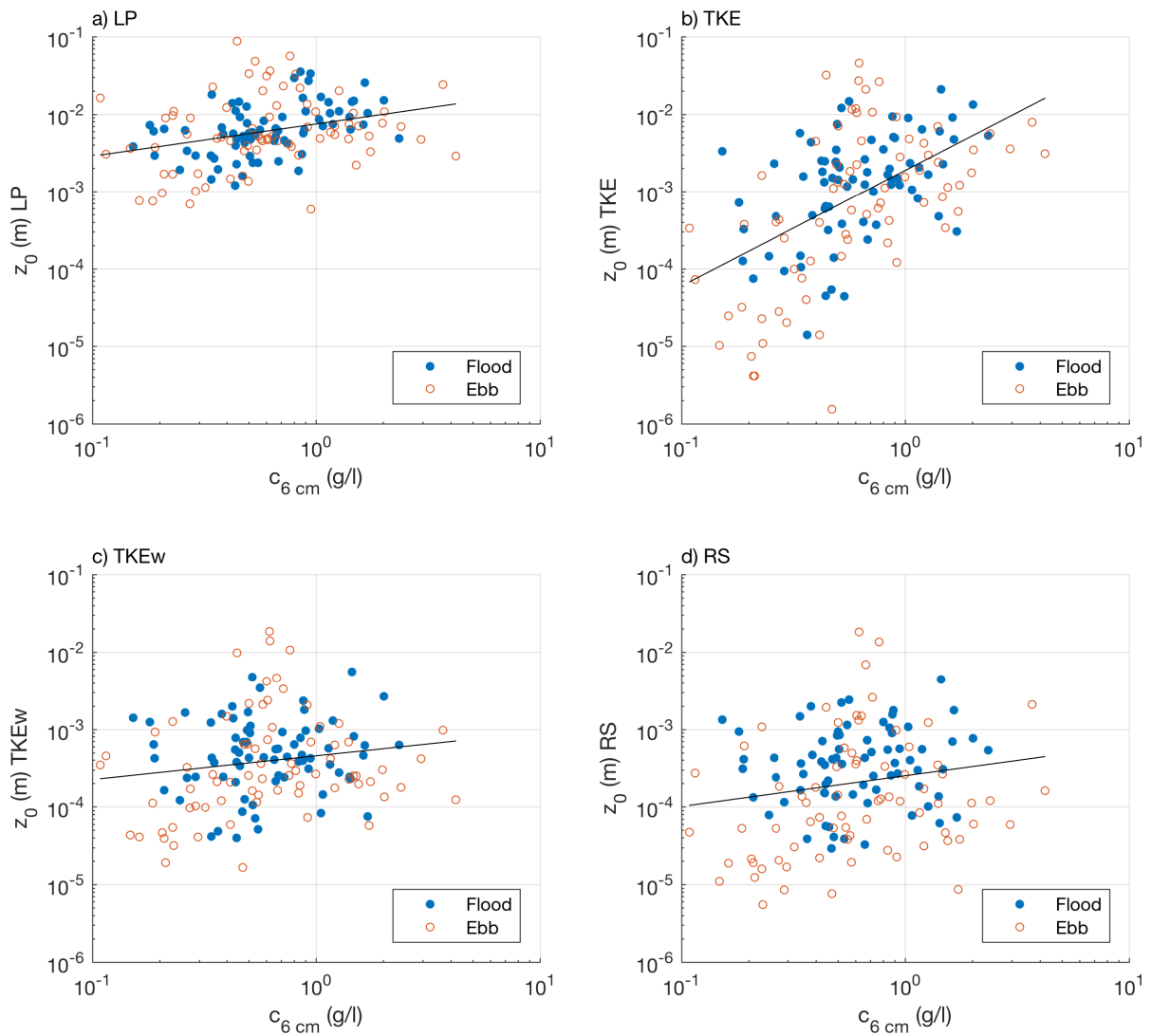


Figure 3.7 Roughness length based on (a) LP method (b) TKE method (c) TKEw method and (d) RS method as a function of measured concentration of SPM at 6 cm above bed. The solid line drawn in each panel, represents a trendline using the least squares method.

3.2 Modeling

From the statistical analysis in § 3.1.4 the suggestion was raised that the measured suspended sediment is not governed primarily by advection, but by local resuspension. Wind at the surface, together with tidal flow, could be responsible for resuspension and increasing suspended concentration, which at the same time hinders the development of fluid mud or consolidation of a mud layer on the bed. Hence, making the sediment rougher at the bed. The effect of fluid mud formation on hydraulic roughness is investigated using a 1DV numerical model. A series of simulations are performed divided into simulations with stationary conditions and with non-stationary conditions. In the simulations, a collapse in the concentration profile will be investigated since this could indicate the formation of a fluid mud layer (Winterwerp, 2001). This is done by modeling multiple simulations with stationary hydrodynamic conditions and investigate for which homogeneous initial concentration a two-layered fluid system is formed. First, the situation for one simulation with stationary conditions is elaborated.

3.2.1 Stationary simulation with $h = 1.6$ m and 0.25 m/s

The situation in fig. 3.8 shows the temporal evolution of the concentration for a simulation imposed with a constant waterdepth of 1.6 m and depth-averaged velocity of 0.25 m/s. The concentration profile collapses when the initial homogeneous concentration is set to at least 0.525 g/l. With a slight increase in the initial concentration, concentrations closer to the bed are higher, indicating a more L-shaped concentration profile (fig. 3.8a). Before the transition from a single-layered fluid system (saturated suspension) to a two-layered fluid system an equilibrium is reached after 40 minutes. When a two-layered fluid system is present (supersaturated suspension) it takes 80 minutes for reaching equilibrium.

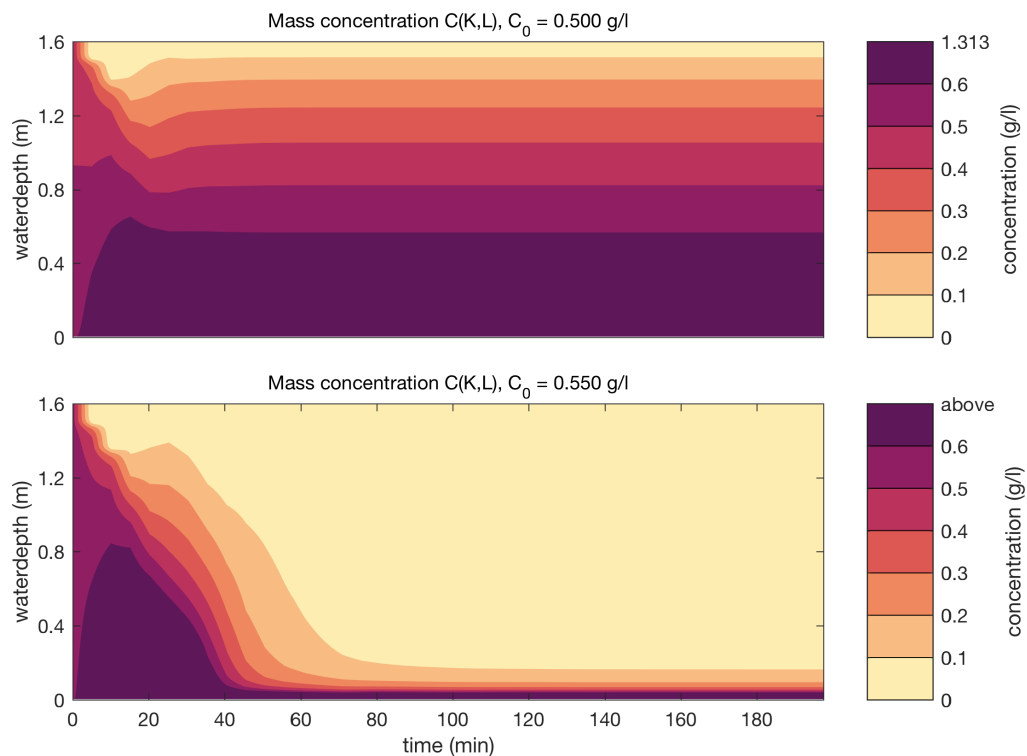


Figure 3.8 Isolutals for (a) saturated suspension and (b) supersaturated suspension for a constant waterdepth h of 1.6m and a constant depth-averaged velocity U of 0.25m/s

As soon as a two-layered fluid system is formed the concentration profile collapses (fig. 3.8). The turbulent energy profile after collapsing shows values which are an order of magnitude smaller than the uncollapsed situations, indicating dampening of the turbulent energy by the fluid mud layer. Furthermore, the eddy viscosity decreases and the vertical viscosity profile differs in shape from the uncollapsed situations. A similar trend is visible for the eddy diffusivity showing a decrease again. Overall, the profiles in fig. 3.11 are in agreement with the criteria described in Winterwerp (2001).

3.2.2 Fluid mud formation for stationary conditions

Stationary simulations are carried out for a series of hydrodynamic conditions based on observed velocities and water depths. For combinations of water depth and velocity the initial concentration is gradually increased until the concentration profile collapses (L-shaped profile as in fig. 3.11). For these simulations, it is assumed there is no water bed exchange.

From the dataset the maximum waterdepth is determined and reaches values up to 2.65 m. The measured velocities reach magnitudes up to 0.7 m/s. For the series of hydrodynamic conditions, the initial homogeneous concentration is gradually increased until a fluid mud layer is formed as exemplified in fig. 3.8. The model parameters for these simulations are described in table 2.5.

The results for all the stationary simulations are put together in a matrix in table 3.2 with on the horizontal the prescribed velocity and the vertical the water depth. A graphical presentation of the matrix is displayed in fig. 3.9. In this figure, the squared symbols indicate for which hydrodynamic conditions (in terms of depth-averaged velocity U and water depth h) simulations were performed for finding fluid mud formation. The solid line encloses the observed water depth and velocity magnitude of the dataset.

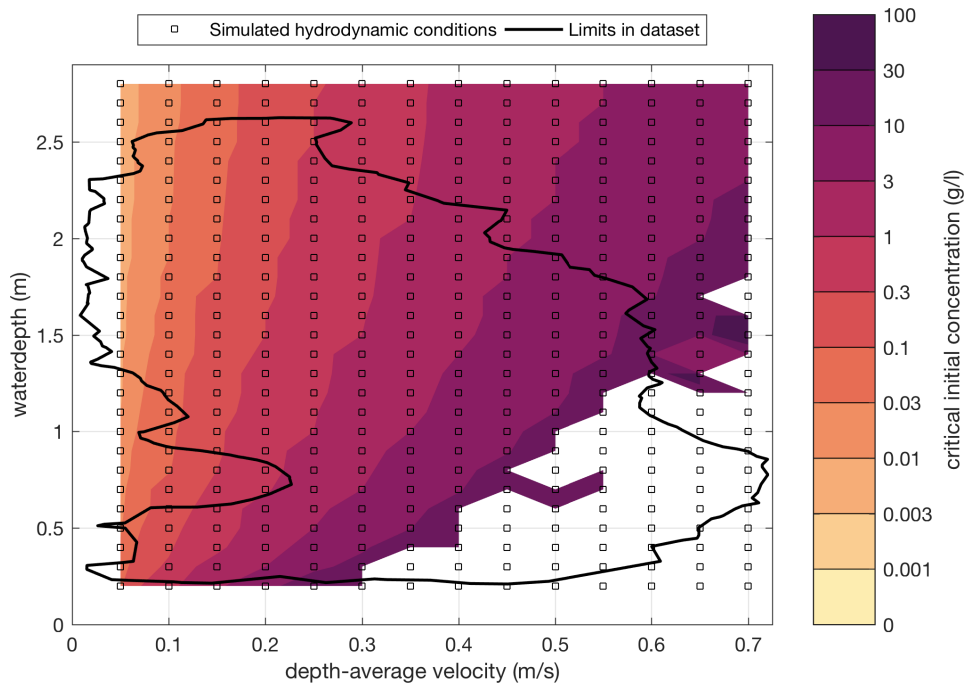


Figure 3.9 Initial homogeneous concentrations above which a two-layered fluid system is formed. The squares indicate for which hydrodynamic conditions the simulations were performed. The solid line indicates the boundaries of the dataset in terms of waterdepth and velocity magnitude.

In fig. 3.9 a white area is visible for velocities larger then 0.3 m/s at low water depths of about 0.5 m. For these combinations, no critical concentration was found for the formation of fluid mud, since the imposed initial concentration is limited to 100 g/L. It can be observed that with increasing water depth (vertical axis in fig. 3.9) a lower initial concentration is required for fluid mud formation. The isolines are more leaning towards the vertical axis instead of the horizontal axis. If they would be of equal importance, the isolines should follow the line $y = x$. For an increasing velocity a higher initial concentration is needed, but compared to the water depth, this concentration needs to be relatively higher. Velocity is, therefore, more important for fluid mud formation then water depth. In the area with small flow velocities (up to 25 cm/s) and a minimum water depth of 0.75 m, inside the boundaries of the dataset, an initial concentration of up to 300 mg/L is required for formation of a fluid mud layer. For higher velocities (above 25 cm/s) and water depths above 1 m, this starts at 1 g/L.

Table 3.2 Critical homogeneous concentrations for fluid mud formation in g/L. On the short axis the waterdepth h from 0.2 to 2.8 m. On the long axis the depth-averaged velocity magnitude U from 0.05 to 0.7 m/s.

	0.05	0.10	0.15	0.20	0.25	0.30	0.35	0.40	0.45	0.50	0.55	0.60	0.65	0.70
0.20	0.08	0.6	2.5	5.5	20.0	25.0								
0.30	0.05	0.35	1.5	3.0	6.5	15.0								
0.40	0.035	0.25	0.75	2.0	4.0	8.0	20.0	15.0						
0.50	0.025	0.2	0.55	1.5	3.0	5.5	10	25.0						
0.60	0.02	0.15	0.45	1.5	2.5	4.0	7.0	15.0						
0.70	0.015	0.15	0.35	0.85	2.0	3.0	5.5	9.0	20.0	15.0	20.0			
0.80	0.015	0.09	0.3	0.7	1.5	2.5	4.5	7.0	15.0		15.0			
0.90	0.015	0.08	0.25	0.6	1.5	2.5	3.5	5.5	9.0	20.0				
1.00	0.01	0.07	0.25	0.55	1.0	2.0	3.0	5.0	7.5	15.0		15.0	20.0	
1.10	0.01	0.06	0.2	0.45	0.9	2.0	2.5	4.0	6.5	10.0	20.0			
1.20	0.008	0.055	0.2	0.4	0.8	1.5	2.5	3.5	5.5	8.0	15.0		15.0	20.0
1.30	0.008	0.05	0.2	0.4	0.7	1.5	2.0	3.5	5.0	7.0	15.0	20.0	50.0	
1.40	0.008	0.045	0.15	0.35	0.65	1.5	2.0	3.0	4.5	6.5	9.0	15.0		15.0
1.50	0.006	0.04	0.15	0.3	0.6	1.0	2.0	2.5	4.0	5.5	8.0	15.0	25.0	45.0
1.60	0.006	0.04	0.15	0.3	0.55	0.95	1.5	2.5	3.5	5.0	7.0	15.0	20.0	50.0
1.70	0.006	0.035	0.15	0.25	0.5	0.85	1.5	2.5	3.5	4.5	6.5	10	15.0	
1.80	0.006	0.035	0.1	0.25	0.45	0.8	1.5	2.0	3.0	4.0	6.0	8.5	15.0	25.0
1.90	0.004	0.03	0.095	0.25	0.45	0.75	1.5	2.0	3.0	4.0	5.5	7.5	15.0	20.0
2.00	0.004	0.03	0.09	0.2	0.4	0.7	1.5	2.0	2.5	3.5	5.0	7.0	10	15.0
2.10	0.004	0.03	0.085	0.2	0.4	0.65	1.0	2.0	2.5	3.5	4.5	6.5	8.5	15.0
2.20	0.004	0.025	0.08	0.2	0.35	0.6	0.95	1.5	2.5	3.0	4.5	6.0	8.0	15.0
2.30	0.004	0.025	0.075	0.2	0.35	0.6	0.9	1.5	2.0	3.0	4.0	5.5	7.5	10.0
2.40	0.004	0.025	0.07	0.2	0.35	0.55	0.85	1.5	2.0	3.0	4.0	5.0	7.0	10
2.50	0.004	0.025	0.065	0.15	0.3	0.5	0.8	1.5	2.0	2.5	3.5	4.5	6.5	8.5
2.60	0.004	0.02	0.065	0.15	0.3	0.5	0.75	1.5	2.0	2.5	3.5	4.5	6.0	8.0
2.70	0.004	0.02	0.06	0.15	0.3	0.45	0.75	1.5	2.0	2.5	3.0	4.0	5.5	7.5
2.80	0.004	0.02	0.06	0.15	0.25	0.45	0.7	1.5	1.5	2.5	3.0	4.0	5.5	7.0

3.2.3 Roughness calculation for simulation with stationary conditions

For the simulation with a water depth of 1.6 m and 0.25 m/s the LP method is applied to obtain roughness length z_0 . In fig. 3.10 the determination of the roughness z_0 is plotted against the initial concentration together with the goodness of fit from the logarithmic fit. It can be concluded that the roughness increases towards the critical concentration, but as soon as the critical concentration is reached and the concentration profile collapses, the roughness decreases. When the concentration approaches the critical concentration the velocity profile deviates more and more from a logarithmic profile.

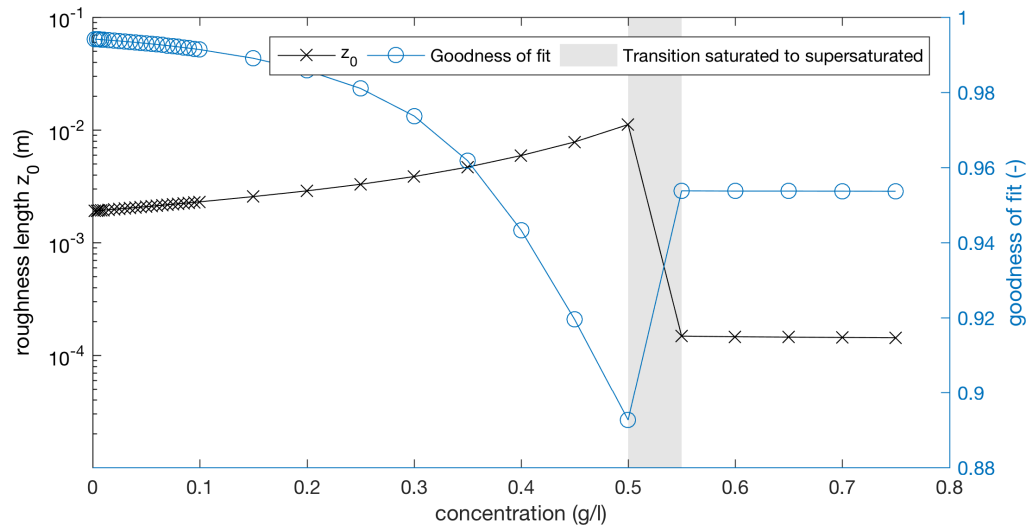


Figure 3.10 Roughness length z_0 based on LP method applied on velocity profiles for simulation with stationary water-depth of 1.6 m and 0.25 m/s. The grey area indicates the transition from saturated to a supersaturated condition.

The time to reach equilibrium conditions increases with depth (fig. 3.12) and velocity (appendix B). When the period needed to reach equilibrium approaches tidal timescales, equilibrium may in reality never be reached. Therefore, the next section evaluates the effect of time-varying boundary conditions.

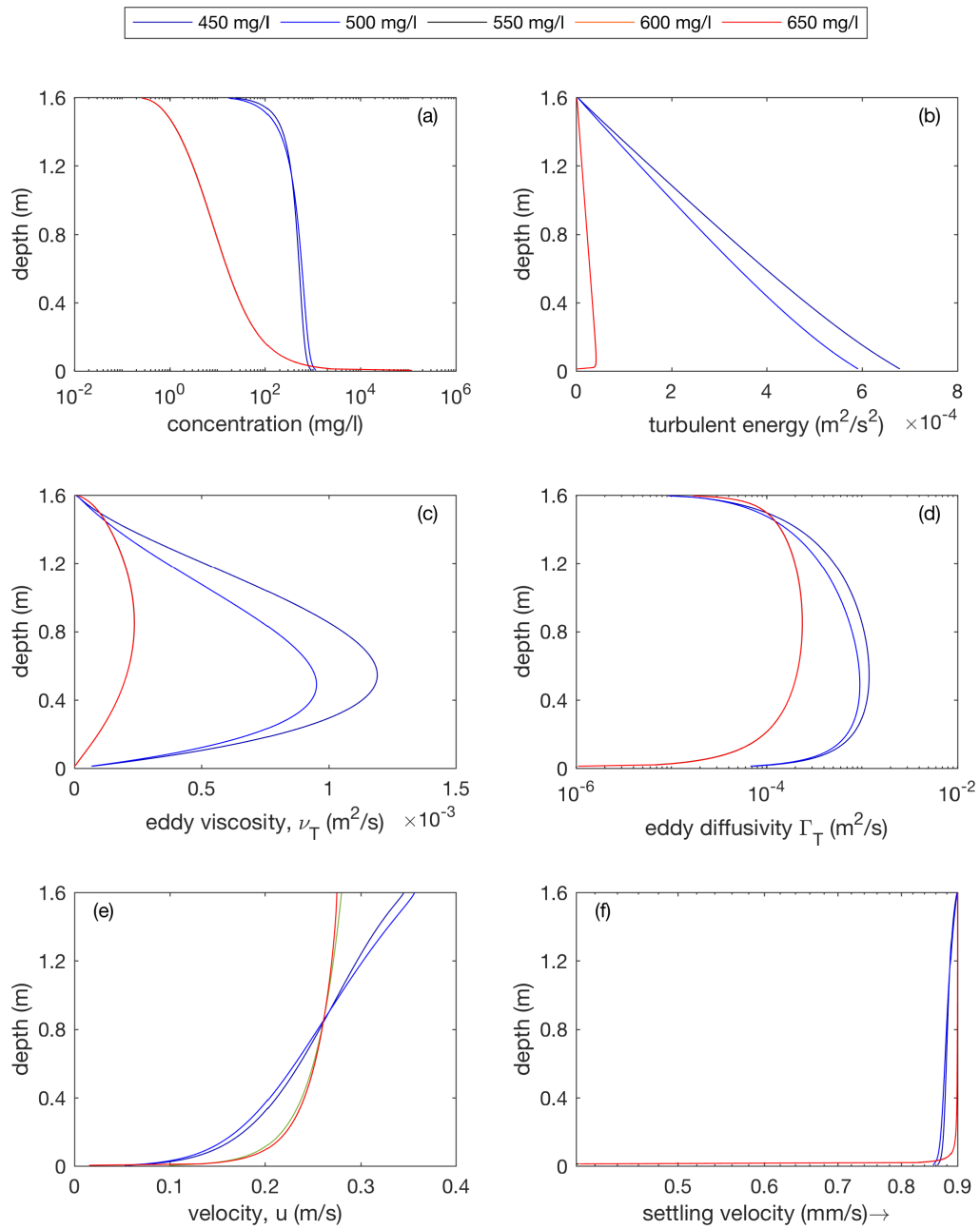


Figure 3.11 Vertical profiles of (a) concentration (b) turbulent energy (c) eddy viscosity (d) eddy diffusivity (e) velocity and (f) settling velocity for stationary simulation with water depth $h = 1.6$ m and depth-averaged velocity $U = 0.25$ m/s. The black lines represent the profiles for which fluid mud has formed whereas the blue lines represent a saturated situation. When the concentration increases the lines start overlapping with the supersaturated situation.

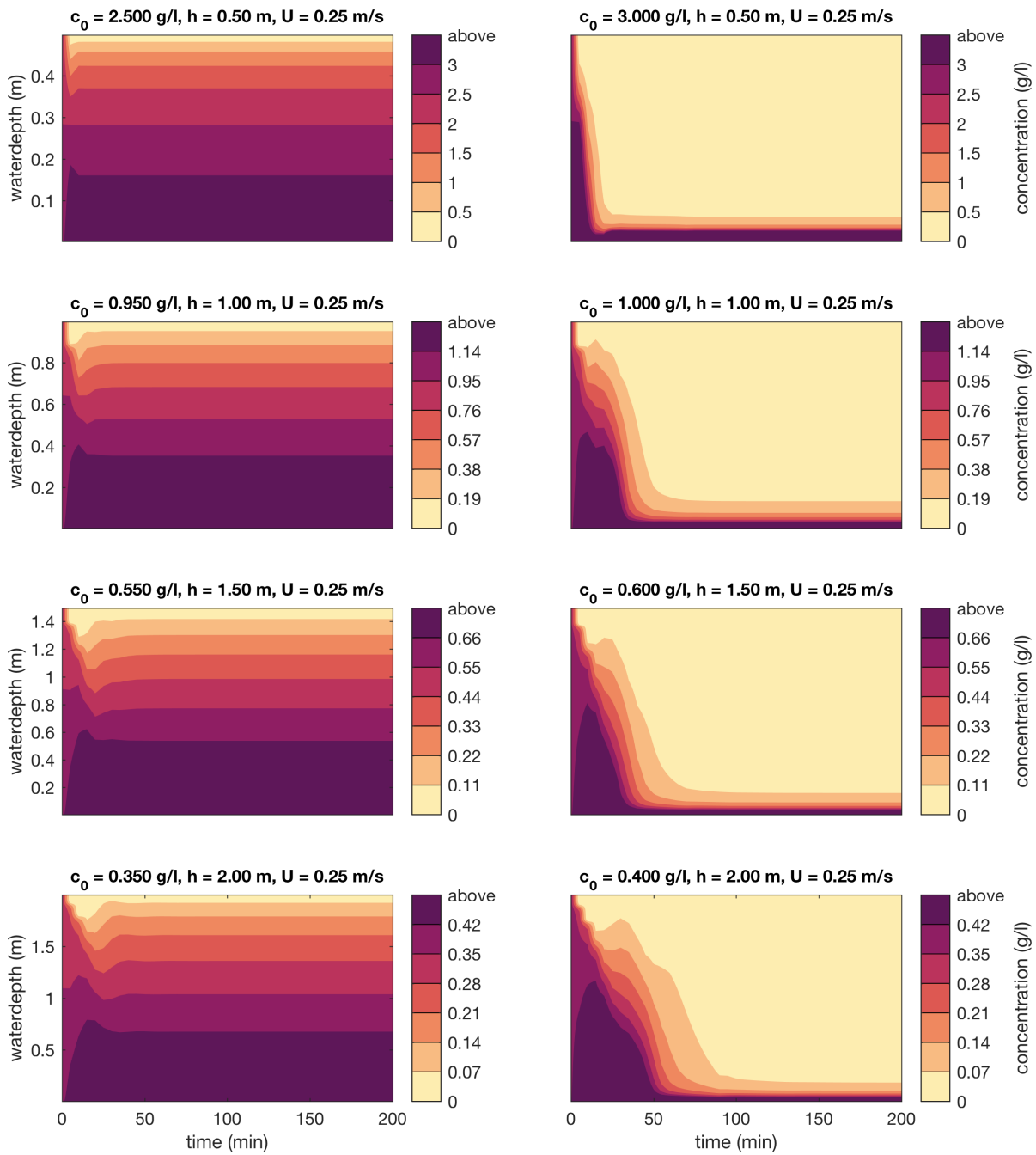


Figure 3.12 Initial homogeneous concentrations for which the concentration profile collapses for a depth-averaged velocity of 0.25 m/s.

3.2.4 Simulations with transient conditions

Simulations with non-stationary conditions are conducted with similar model parameters as for the simulations with stationary conditions. The simulation is carried out with water depth and velocity of one tidal cycle around 7th May starting at low water. The simulation is performed without meteorological forcing (wind and waves). In fig. 3.13 input time-series of waterdepth and depth-averaged velocity are shown.

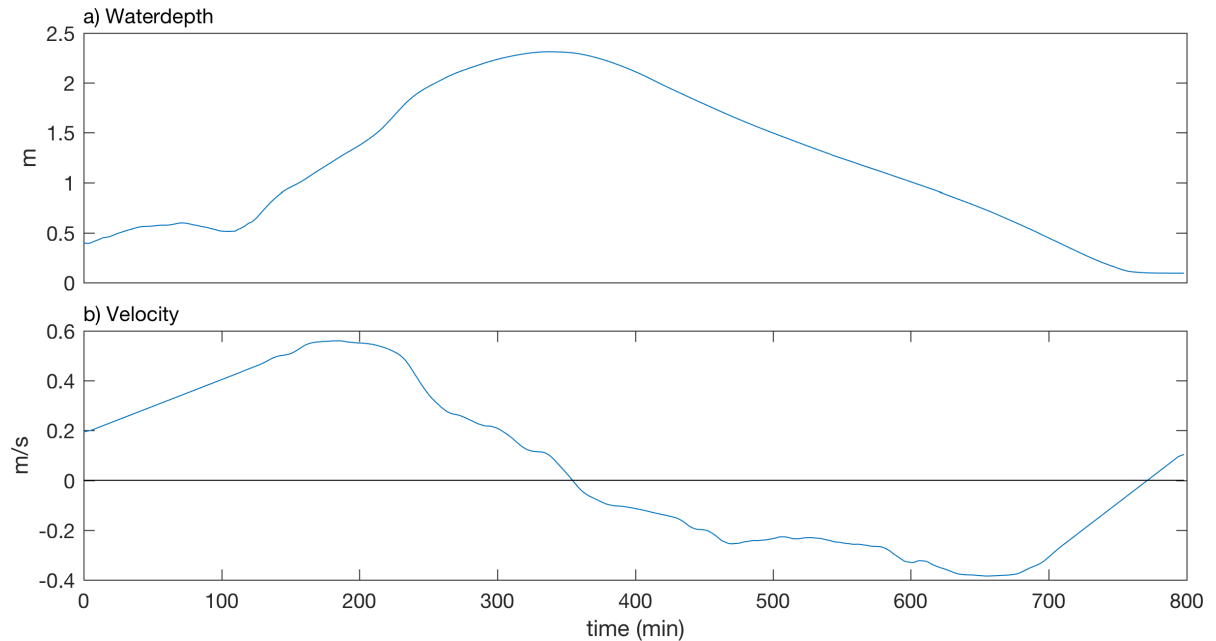


Figure 3.13 Input timeseries of (A) waterdepth and (B) velocity for simulation with one tidal cycle.

The simulation is performed with an initial concentration of 0.4 g/L. The mass concentration during the tidal cycle is displayed in fig. 3.14. In fig. 3.15 the roughness is calculated from the velocity profiles using the LP method. The roughness together with the goodness of fit is shown. During the turn of the tide, the goodness of fit r^2 is low. When r^2 is below 0.75, the roughness is not calculated. Looking at fig. 3.14 and fig. 3.15 the roughness increases towards the turn of the tide. The concentration profile becomes L-shaped. After the turn of the tide the concentration profile is still L-shaped, but now the roughness is lowered. After a certain time (500 minutes), the combination of water depth and velocity are sufficient to change the concentration profile from an L-shaped profile to a homogeneous profile, indicating a fluid mud layer. It can be concluded that during a tidal cycle the timescales are short enough for fluid mud formation.

To provide further proof of the conclusion that during a tidal cycle, fluid mud can be formed under certain conditions, the profiles of the concentration, turbulent energy, eddy viscosity and the velocity are displayed in fig. 3.16 for minutes 200, 300, 400 and 500. Minute 200 shows a concentration profile which is homogeneous indicating no collapse in the concentration profile. Besides that, the turbulent energy is increasing towards the bottom. Minutes 300, 400 and 500 show collapsed concentration, turbulent energy and viscosity profiles, which is in agreement with the criteria described in § 1.2.

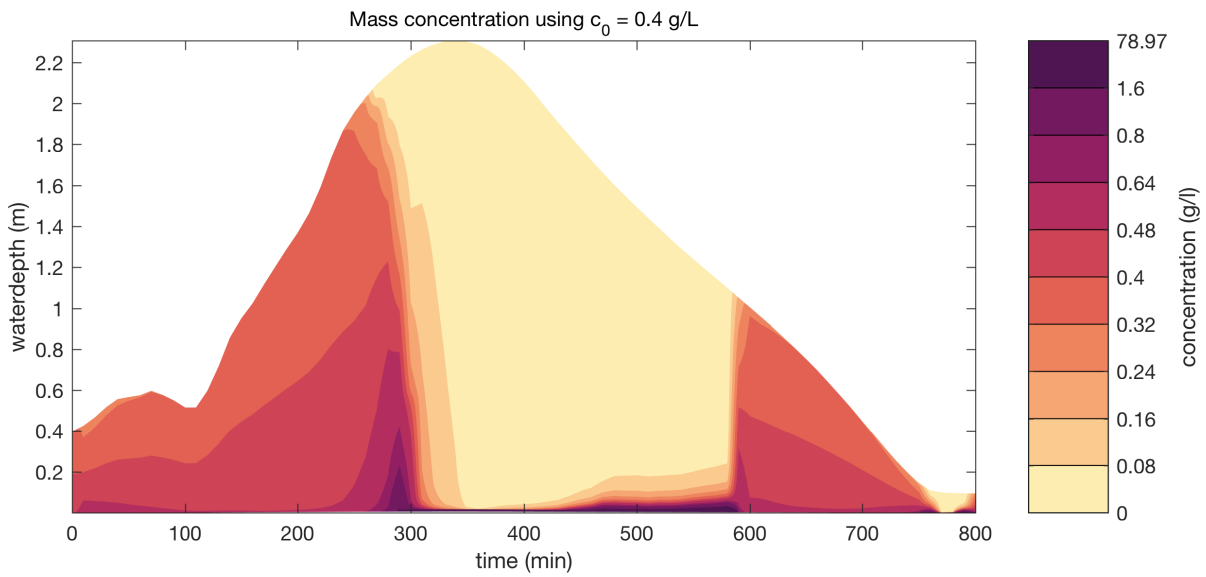


Figure 3.14 Mass concentration for simulation during one tidal cycle.

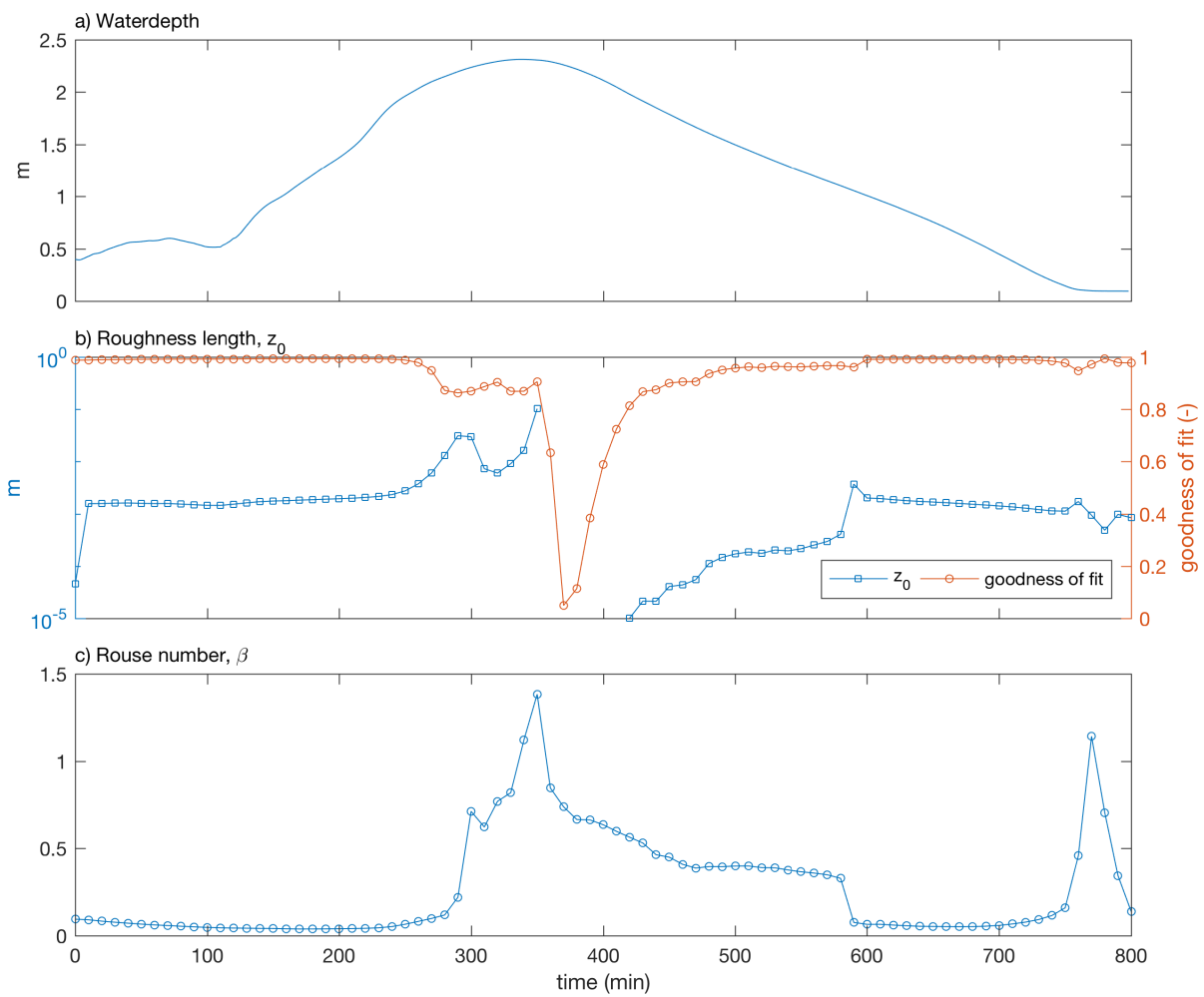


Figure 3.15 (a) Waterdepth (b) roughness length z_0 and (c) Rouse number β for simulation of one tidal cycle.

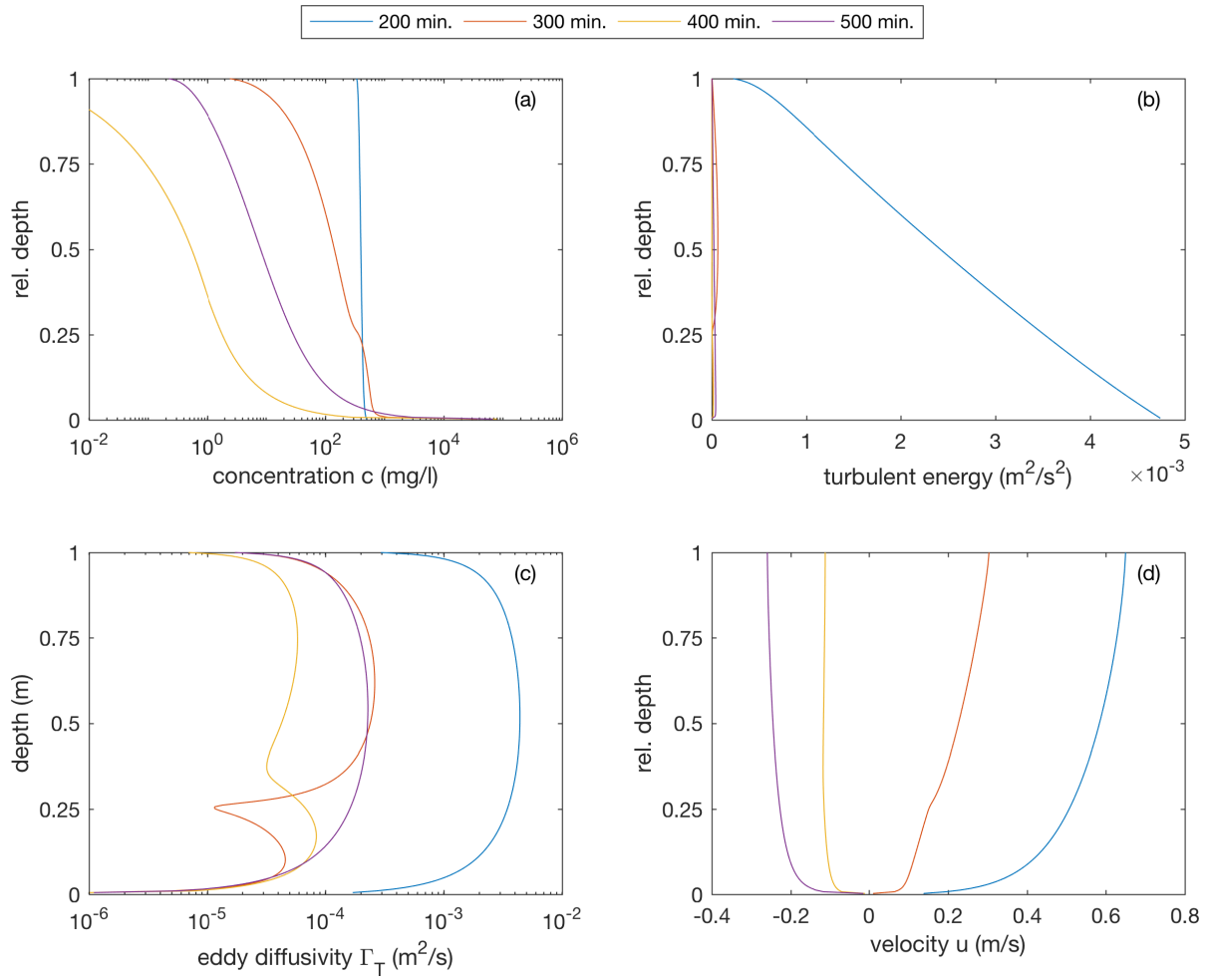
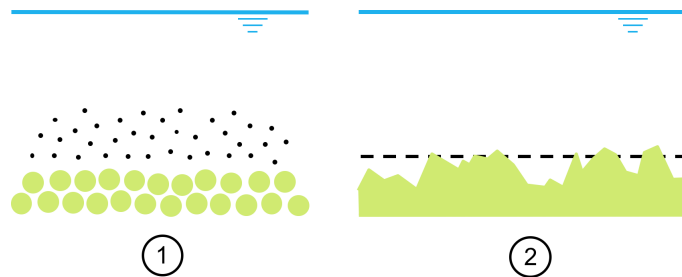


Figure 3.16 Profiles of (a) concentration (b) turbulent energy (c) eddy viscosity and (d) velocity for simulation of one tidal cycle after 100, 200, 300 and 400 minutes. The vertical axis shows the depth relative to the maximum depth at that moment.

4

Discussion

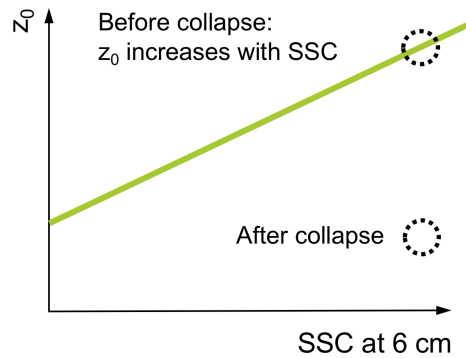
In the introduction, the question was raised which mechanism could cause variability in bed roughness. The approach which was followed consisted of an analysis of field measurements from which the roughness length is being calculated using four bed shear stress methods. The processed data showed intertidal variation in roughness length. Two mechanisms were proposed for the variability in bed roughness. These mechanisms were investigated using statistical analysis and a numerical modeling study.



- All methods assume measurements being performed in the constant stress layer, the region where the logarithmic velocity profile is valid. Furthermore, the log-layer is only valid in idealized situations, i.e., when a fully turbulent boundary layer is formed. When waves are present, this might not always be the case, and other techniques should be used. In this study, it is attempted to circumvent these criteria by setting a minimum to the goodness of fit of the velocity profile. For deriving bed shear stress, a numerical model could have been used to incorporate the presence of waves by implementing wave-current interaction models such as the Grant-Madsen model (Lacy et al., 2005).
- The statistical analysis showed that averaged roughness length per tidal phase increases with suspended sediment concentration at 6 cm above the bed (fig. 3.7). It also showed intertidal (fig. 3.4) and intratidal variations (fig. 3.3). The result of the statistical analysis implies the first mechanism to be correct. However, the sediment characteristics are uniform which makes this mechanism less plausible.
- The intertidal and intratidal roughness length both differ in order of magnitude. The average roughness length per tidal phase is estimated using a geometric mean, which could result in a higher average if there is a large spread. The intratidal variation is in order of magnitude larger towards slack water. The average could be improved using stricter flow criteria which have to be included in the average, i.e., a minimum absolute velocity. There is a intertidal variation, irrespective of the uncertainty in the method for calculating the average (fig. 3.5).
- In order to find under which conditions a fluid mud layer can be formed, simulations with a 1DV numerical model were conducted, with stationary and time-varying boundary conditions. For simulations with stationary conditions, the roughness length decreases as soon as fluid mud has been formed. Towards the critical point - where no fluid mud has formed yet - the roughness

increases with concentration (fig. 3.10). The increase in roughness could be artificial since the velocity profile starts to deviate more and more from a logarithmic profile towards the critical point.

- The numerical model study tested the second mechanism. The model might not be realistic because water-bed exchange is not included. This means that the filling of the rough bed by fluid mud is not modeled. Furthermore, bed irregularities and bedforms are merged into one artificial parameter, whereas Houwman and van Rijn (1999) use bedform models and wave-current models to calculate the roughness.
- As previously stated, from the numerical model study it was found that the roughness length increases with suspended sediment concentration, however, this could be a numerical effect. As can be concluded from the results of the model, the roughness length decreases after a collapse in concentration profile occurs. The result of the numerical model implies the second mechanism to be correct. A decrease in roughness was not observed in the data set contrary to what was expected. This implies that a fluid mud layer is formed below the height at which the OBS had been measuring. So basically, the data set is insufficient to measure very low roughness together with high concentration. A sonar system capturing images of the bed could be used to support this hypothesis.



5

Conclusions

- From the statistical analysis, it can be concluded that the sediment concentration per tidal phase (fig. 3.5) is an order two autoregressive process. Hence, the concentration at time t can be modeled as a function of concentration at time $t-1$ and $t-2$ with additional information on the wind speed. Physically, this means that the sediment concentration increases as a function of the wind speed.
- Averaged roughness length z_0 per tidal phase can be described as concentration of SPM at 6 cm. As a result of this increasing of SPM the bed roughness also increases. This implies that suspended sediment is not primarily governed by horizontal advection, but by local resuspension. During high wind situations, there is more stirring of sediment which leads to resuspension of the bed material.
- From the simulations with stationary conditions it can be concluded that for fluid mud formation, a higher concentration of SPM is required when the velocity becomes larger and water depth lower. With small velocities, the initial concentration is expected to be around 100 mg/L and with higher velocities (up to 30 cm/s), 1 - 10 g/L is required. This shows that the velocity has a more substantial influence than the water depth. A simulation with a constant velocity, the time to reach an equilibrium increases when the water depth increases. The sediment particles have to travel a larger distance to arrive at the lower parts of the water column.
- The roughness increases with increasing concentration of SPM. This is in agreement with the result derived from the statistical analysis. However, as soon as the initial concentration reaches a specific value in which a two-layered fluid system is formed, the roughness decreases significantly and continues to stay low. When this happens, the vertical profile for turbulent energy collapses as well, which indicates damping effect of the turbulence. If this turbulent energy is converted to a shear velocity u_* , this would probably lead to a lower roughness based on the turbulent kinetic energy methods.
- From the simulations with time-varying boundary conditions, it can be concluded that fluid mud can indeed be formed during a tidal cycle using the specific model parameters described in § 2.4.1. During the tidal phase the bed roughness increases towards the turning of the tide; after the turn of the tide, the bed roughness decreases. The concentration profile during flood phase shows no collapse what can be further argued by an increasing turbulent energy from the water surface to the bottom. However, during the ebb phase, the concentration profiles are L-shaped and a decrease in turbulent energy near the bed. Which is in agreement with the criteria described by (Winterwerp, 2001) for the fluid mud formation.

6

Recommendations

- The results from the model simulations could be further investigated and verified by looking at the dataset again. The ADCP instrument gives amplitude signals through which suspended sediment concentration could be measured. The amplitude signal of the ADCP instrument could add extra information on the analysis of the simulation of a tidal cycle.
- The setup of the ADCP instrument can be improved to give a better estimate for the velocity profile. For example by using a setup of single and multiple ADCP instruments measuring over the full water column with high resolution. The amplitude signal of the ADCP can then be related to the concentration of SPM leading to a more indicative profile of concentration of SPM. With this setup, also the influence of wind on the velocity profile in the water column could be investigated. This setup can be investigated in a more controlled environment by doing experiments in the laboratory.
- One conclusion drawn from the statistical analysis is that concentration of SPM is related to bed roughness. By doing more extensive experiments, i.e., in the lab, a better description of this relation could be found. When this is the case, varying roughness can be implemented in numerical models by parameterizing the roughness as a function of concentration of SPM in a custom module.
- The second mechanism involving fluid mud formation can be further investigated using sonar imaging as is also done in Lacy et al. (2005).
- Application of the inertial dissipation method (ID method) as described in (Stapleton and Huntley, 1995) for estimating bed shear stress. This method uses the $k^{-5/3}$ relation between wavenumber (k) and spectral energy (ϕ) within a sub-range of the spectrum to determine turbulence. It is a particularly useful method because the variance of the velocity signal can be separated into fluctuations due to orbital velocities and due to turbulence Soulsby and Humphrey (1989). According Andersen et al. (2007) the orbital velocities and turbulence have to be filtered out from the turbulent kinetic energy which relies on accurate determinations of the inertial subrange. Using the ID method, this can be achieved.



Statistical analysis

This chapter describes the statistical analysis performed on the tidal phase averaged quantities in § 3.1.4. The statistical analysis is performed in R. The figures below describe residuals, autocorrelation as well as results from principal component analysis. The statistical model used is a linear model using generalized least squares.

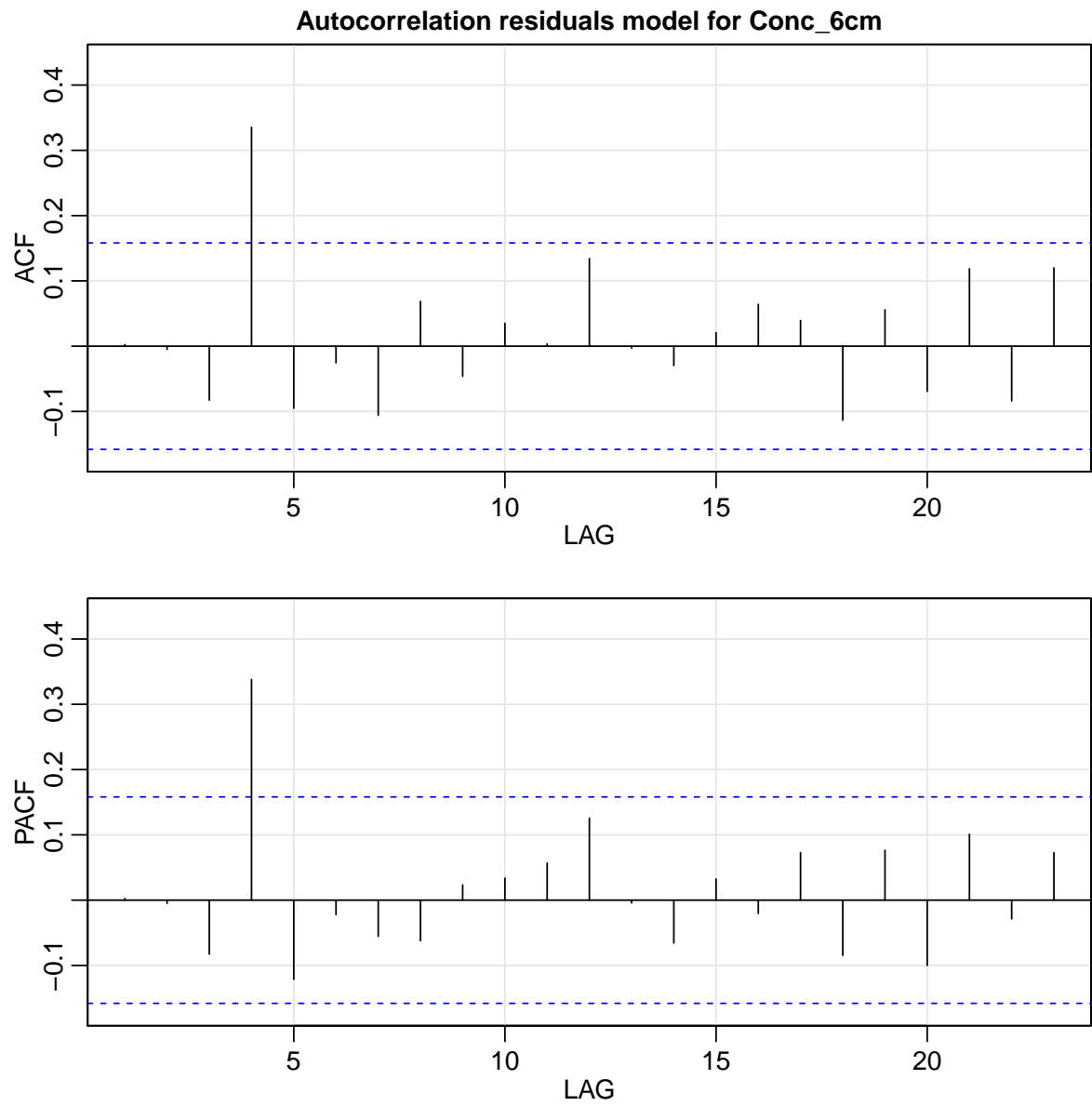


Figure A.1 Autocorrelation residuals from generalized least squares fit described as a linear model between concentration at t , $t-1$, $t-2$ and wind speed

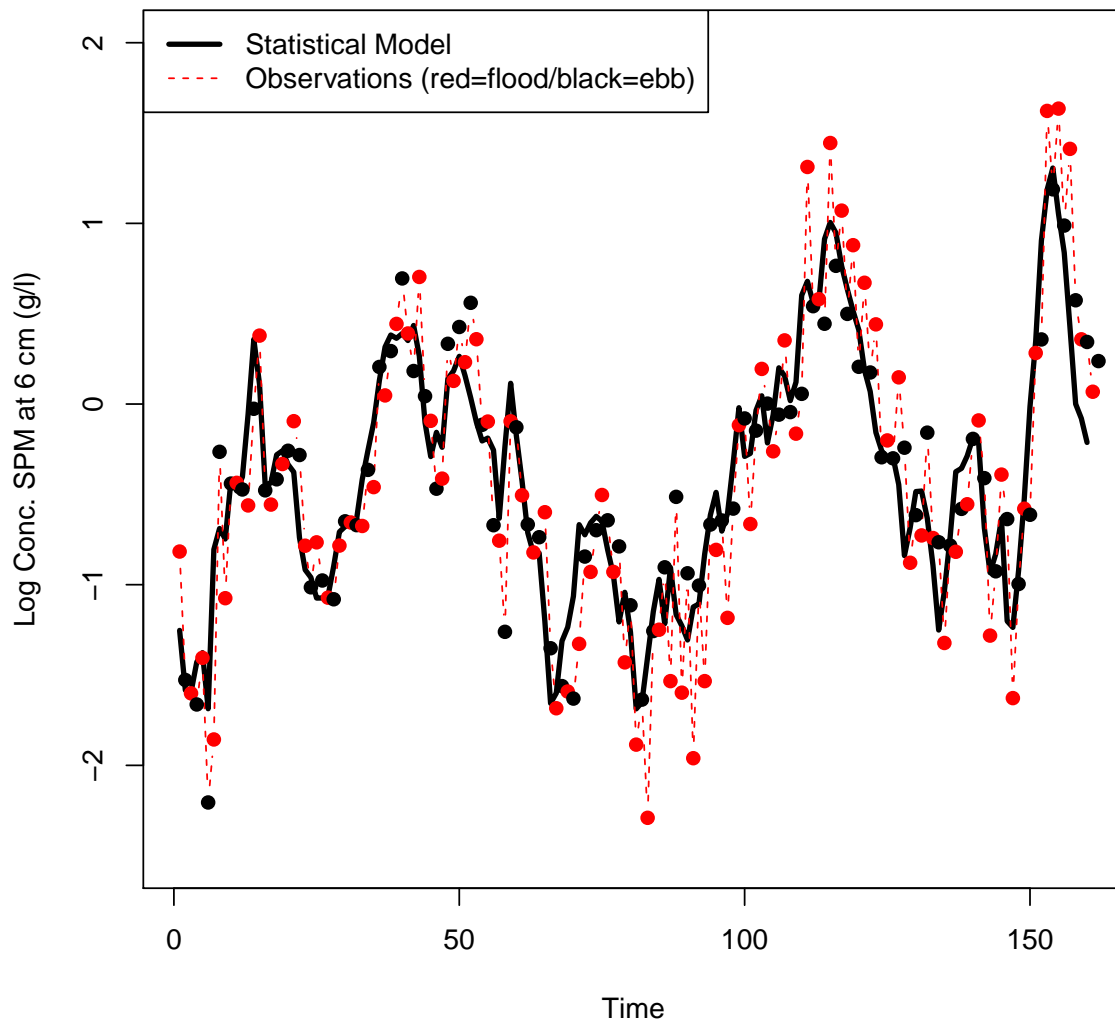


Figure A.2 Time series of the GLS performed in fig. A.1

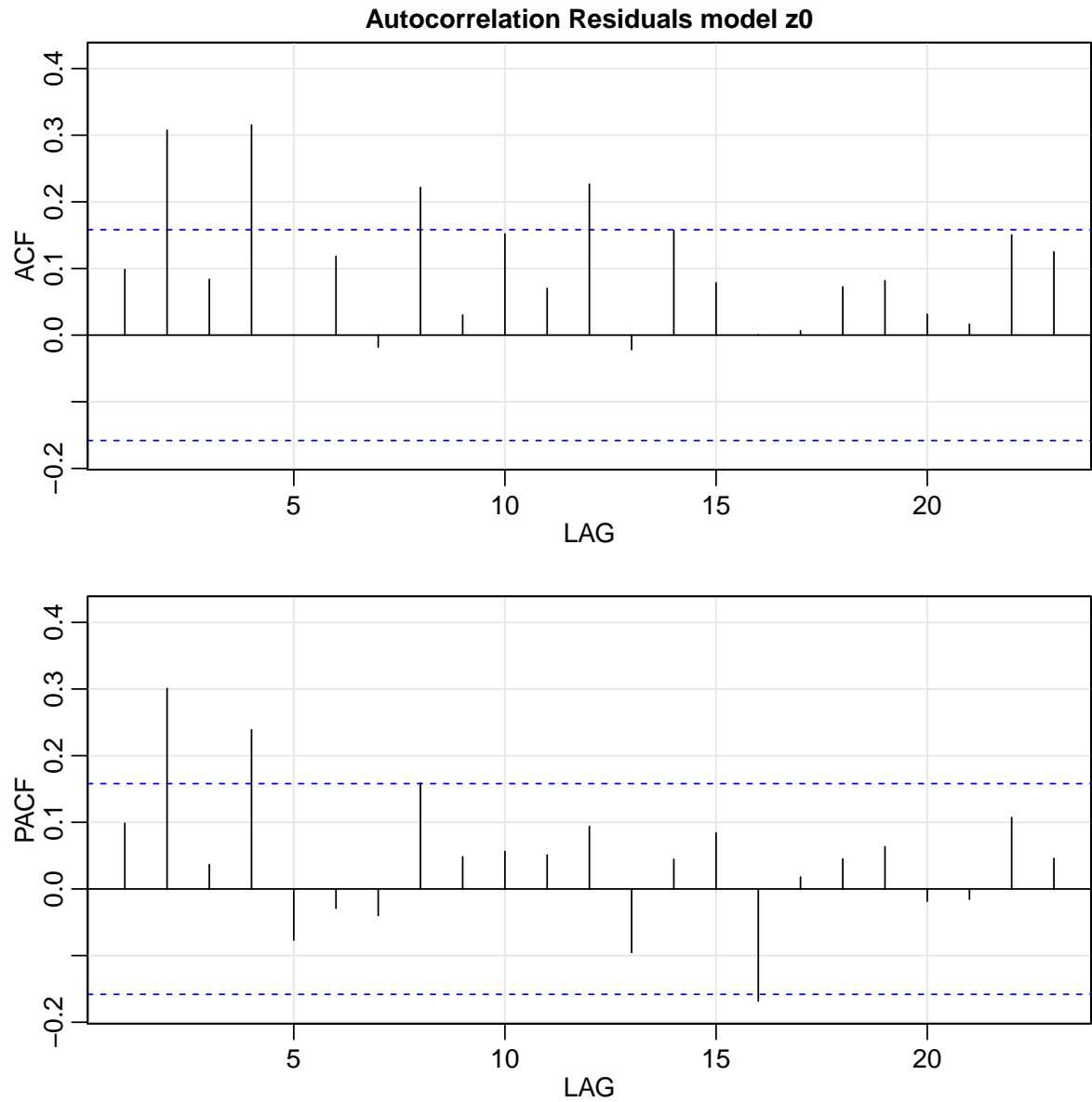


Figure A.3 Autocorrelation residuals from generalized least squares fit described as a linear model between concentration, roughness z_0 based on LP method and maximum current velocity during a tidal phase. A correlation structure reflecting autocorrelation in time is used.

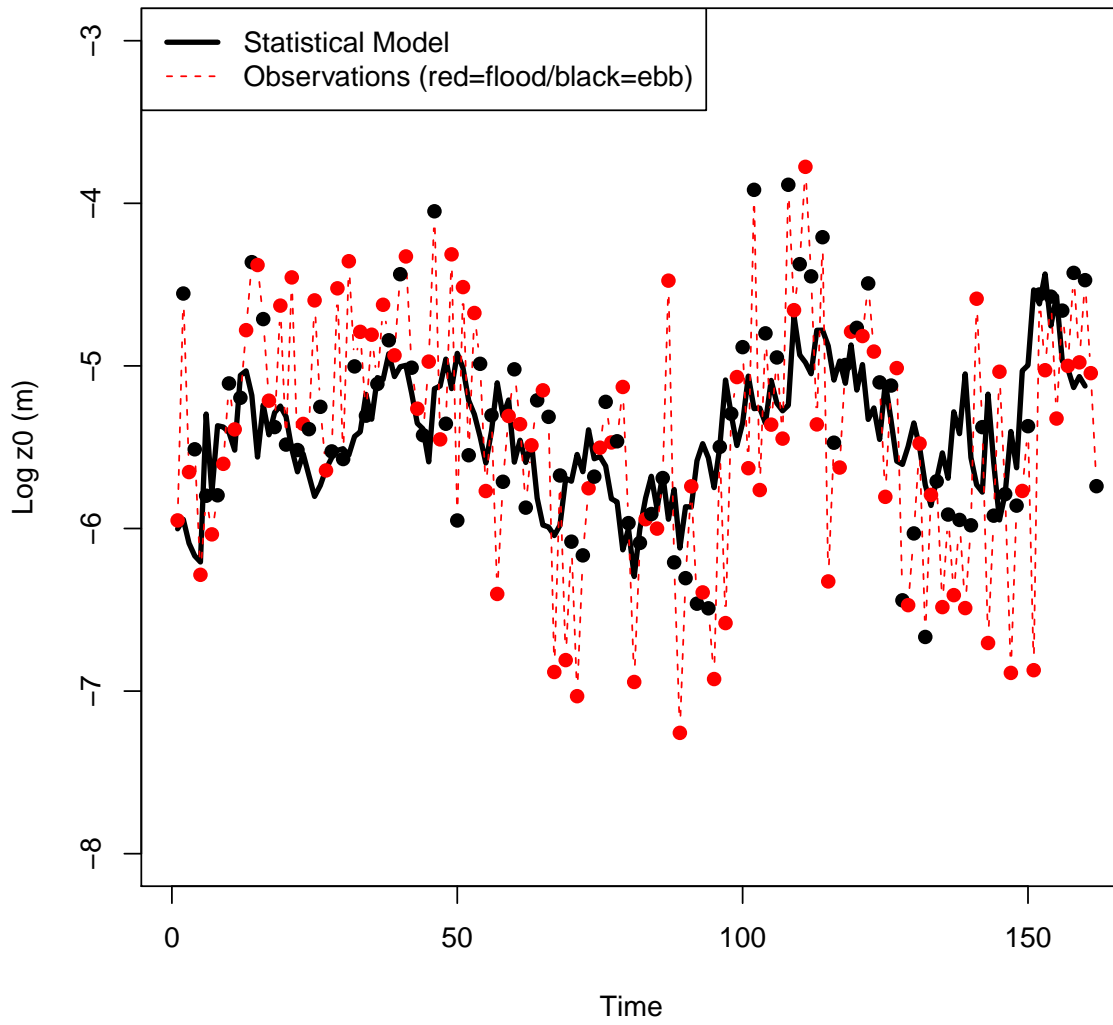


Figure A.4 Time series of the GLS performed infig. A.3

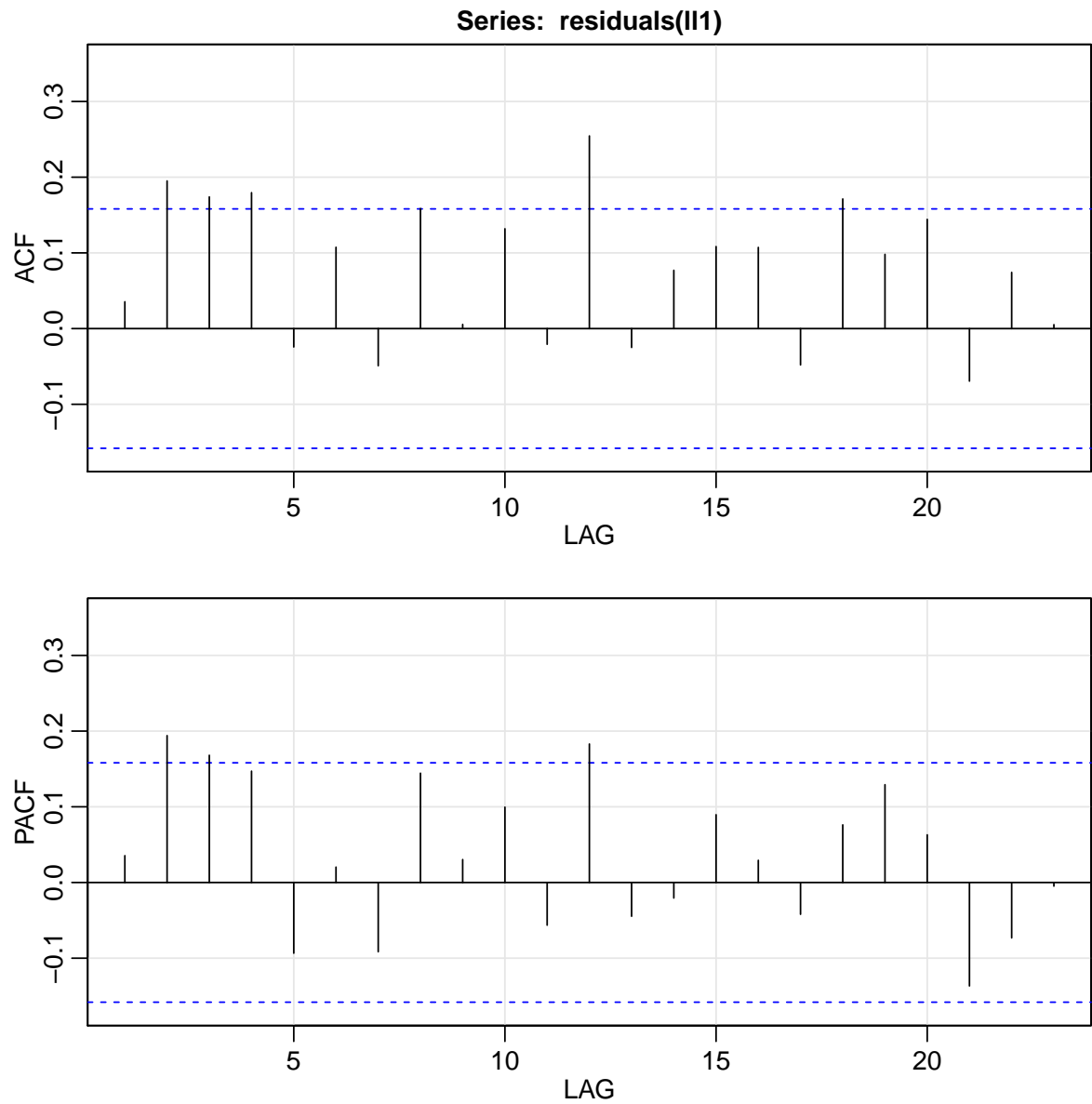


Figure A.5 Autocorrelation residuals from generalized least squares fit described as a linear model between scores of PCA between turbulent kinetic energy methods, wind speed at t , wind speed at $t-1$, wind direction at t and tidal phase.

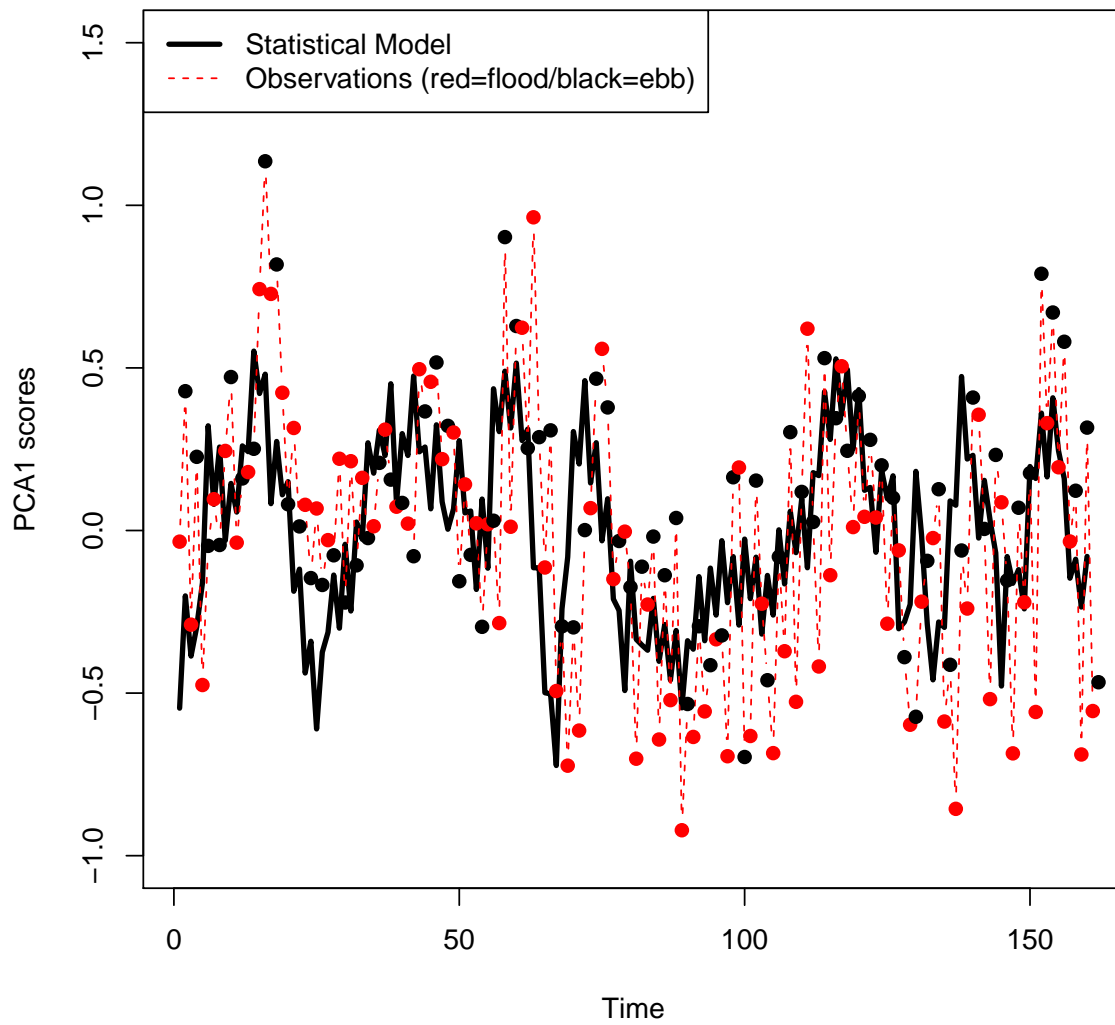


Figure A.6 Time series of the GLS performed in fig. A.5

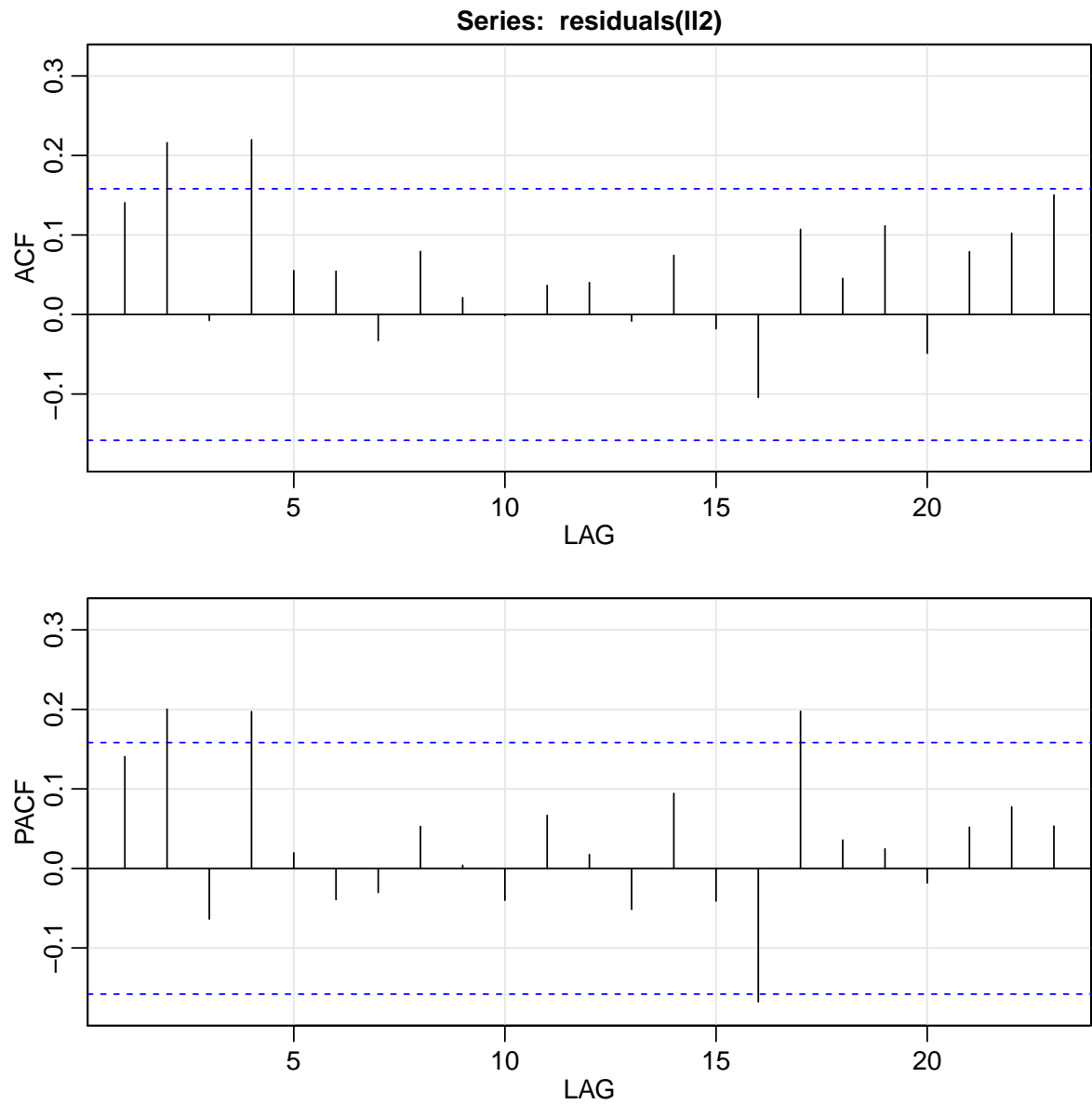


Figure A.7 Autocorrelation residuals from generalized least squares fit described as a linear model between scores of PCA between TKE methods and logarithmic profile method, wind speed, wind direction and concentration

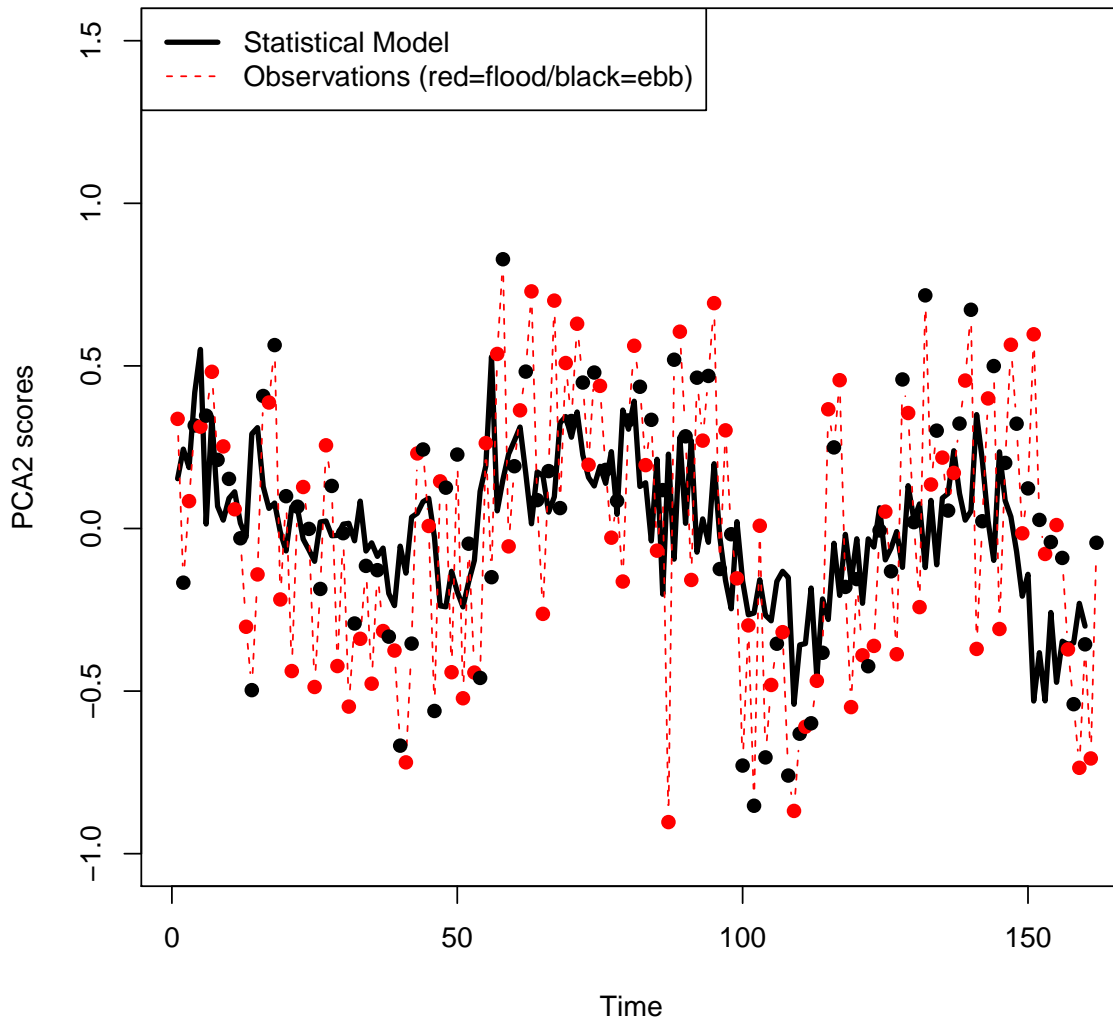


Figure A.8 Time series of the GLS performed in fig. A.7

B

Simulations with stationary boundary conditions

This section shows supplementary results for the 1DV model simulations imposed with stationary conditions.

The transition from saturated to supersaturated conditions for a few hydrodynamic conditions is shown in figs. B.1 and B.5 for velocities of 0.05, 0.25, 0.45 m/s. Collapses are displayed for waterdepths of 0.5, 1.0, 1.5 and 2.0 m. On the left side of the figures, the saturated situation is displayed whereas on the right side the supersaturated.

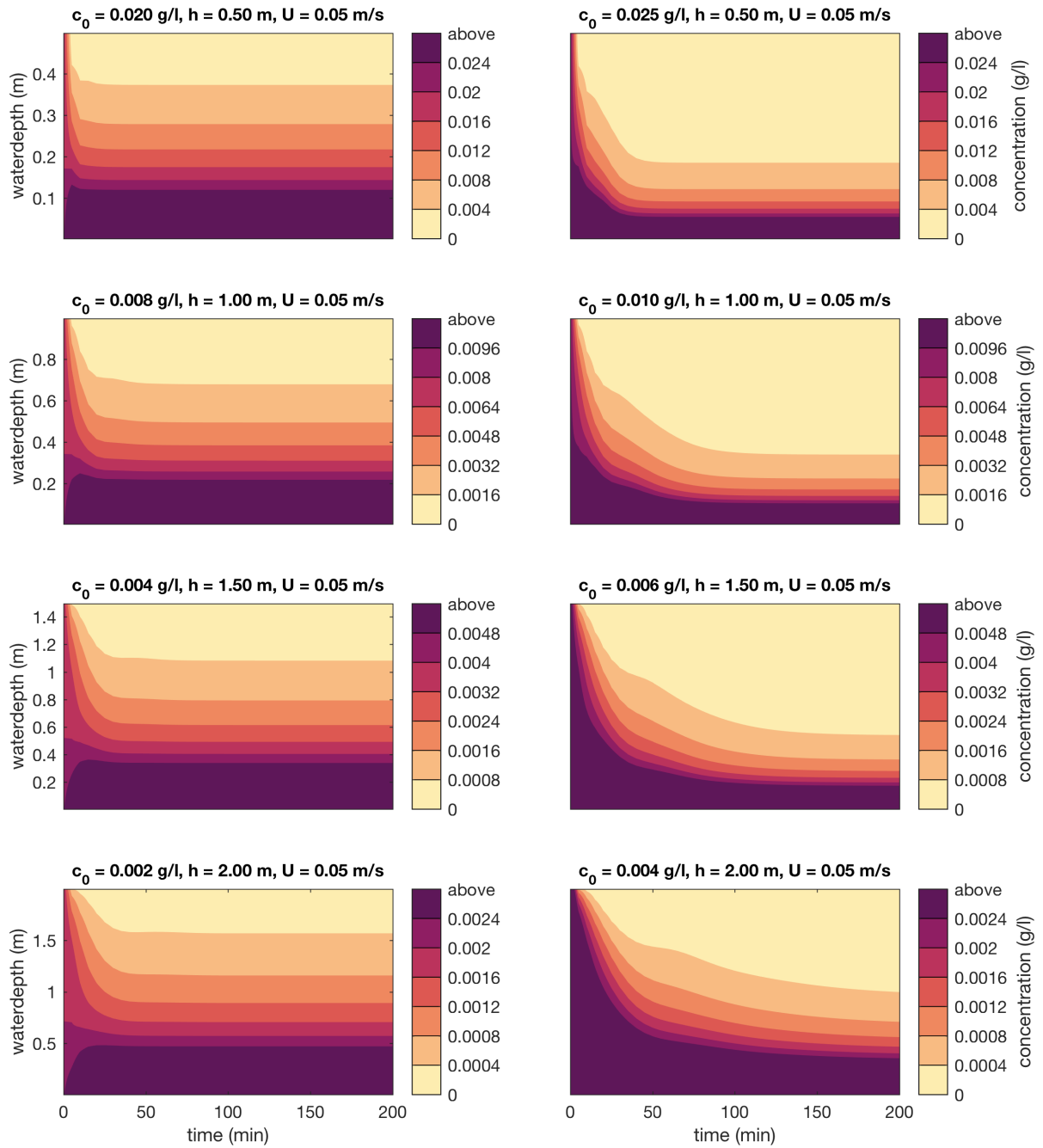


Figure B.1 Initial homogeneous concentrations for which the concentration profile collapses for a depth-averaged velocity of 0.05 m/s.

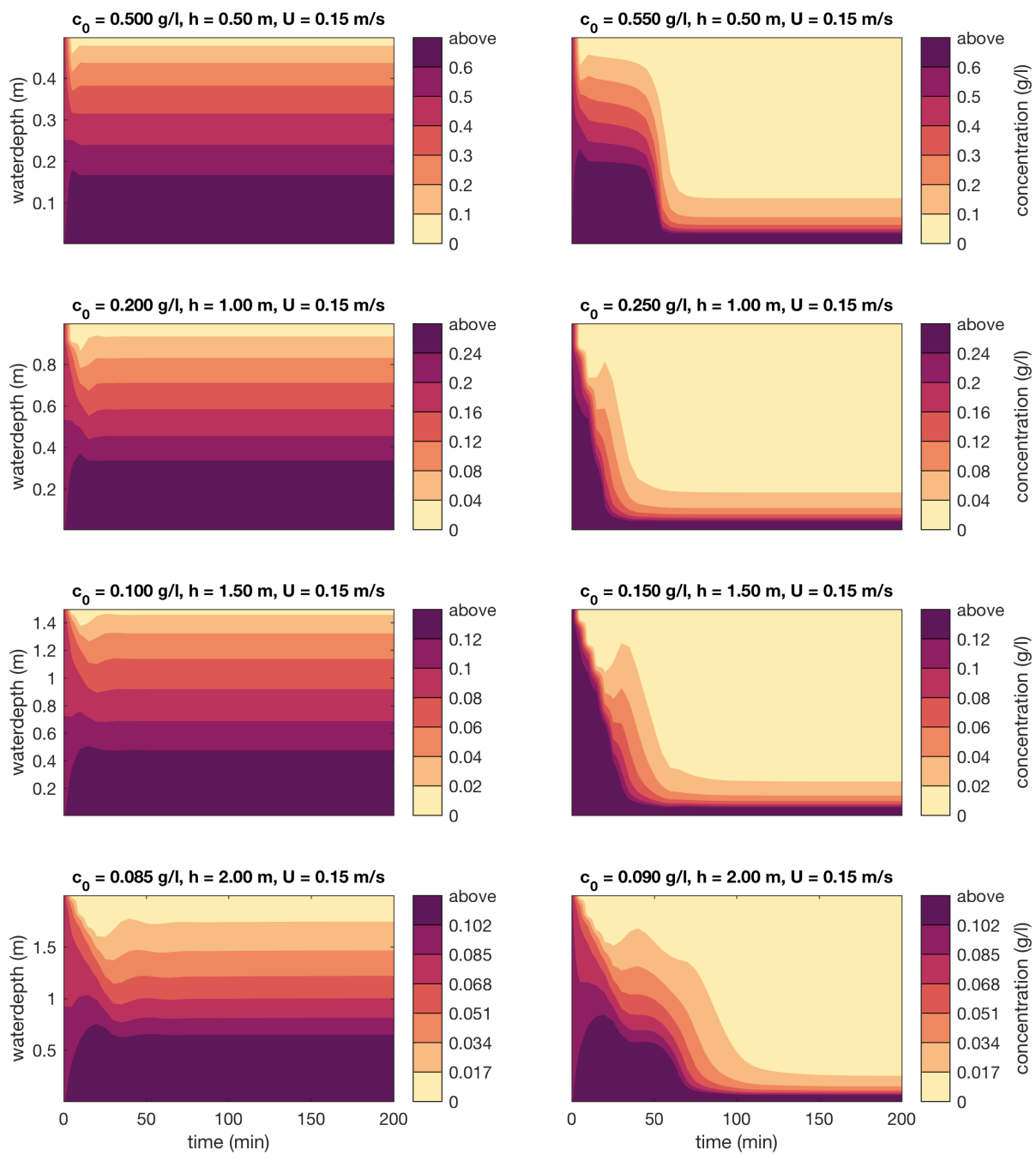


Figure B.2 Initial homogeneous concentrations for which the concentration profile collapses for a depth-averaged velocity of 0.15 m/s.

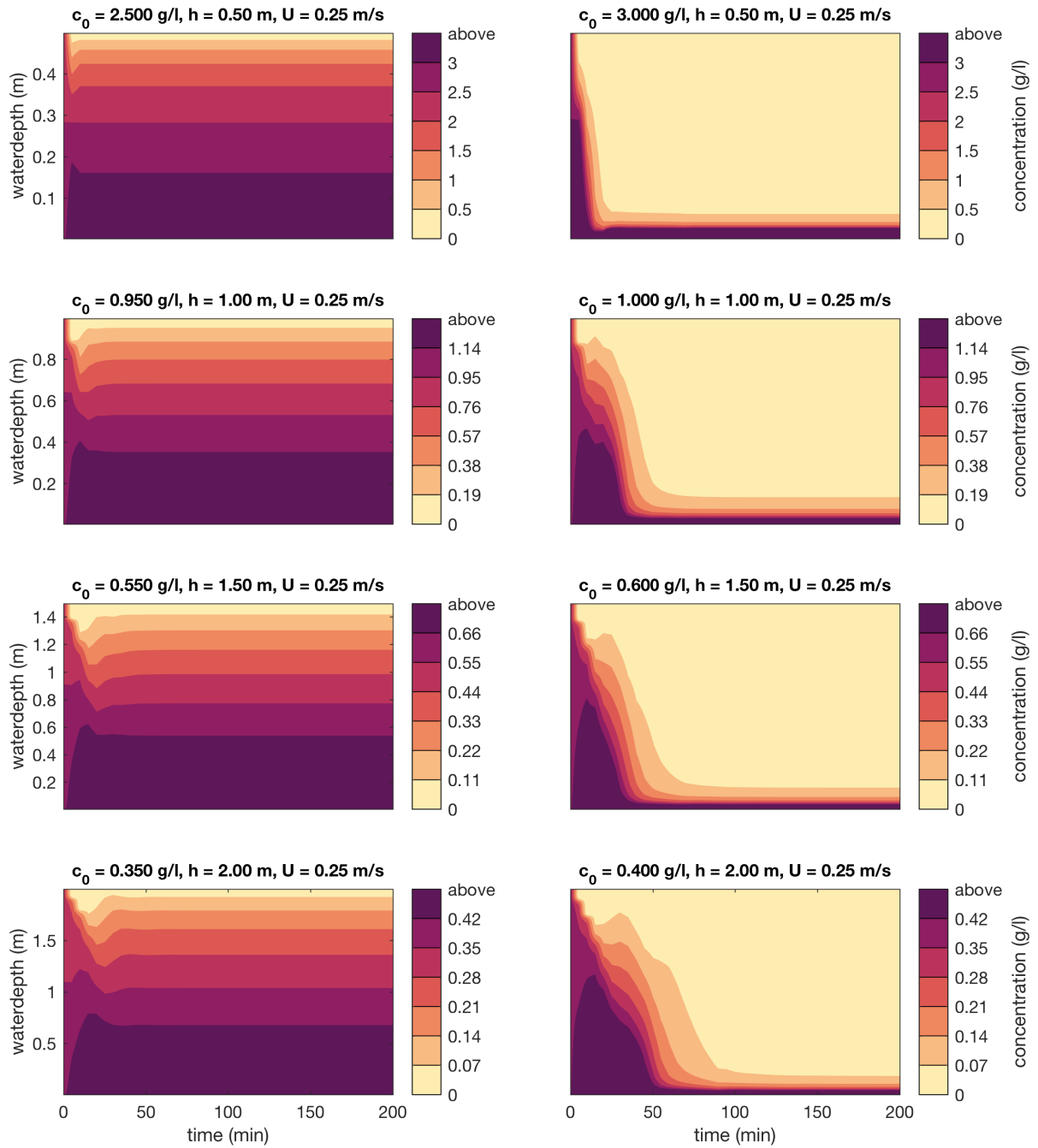


Figure B.3 Initial homogeneous concentrations for which the concentration profile collapses for a depth-averaged velocity of 0.25 m/s.

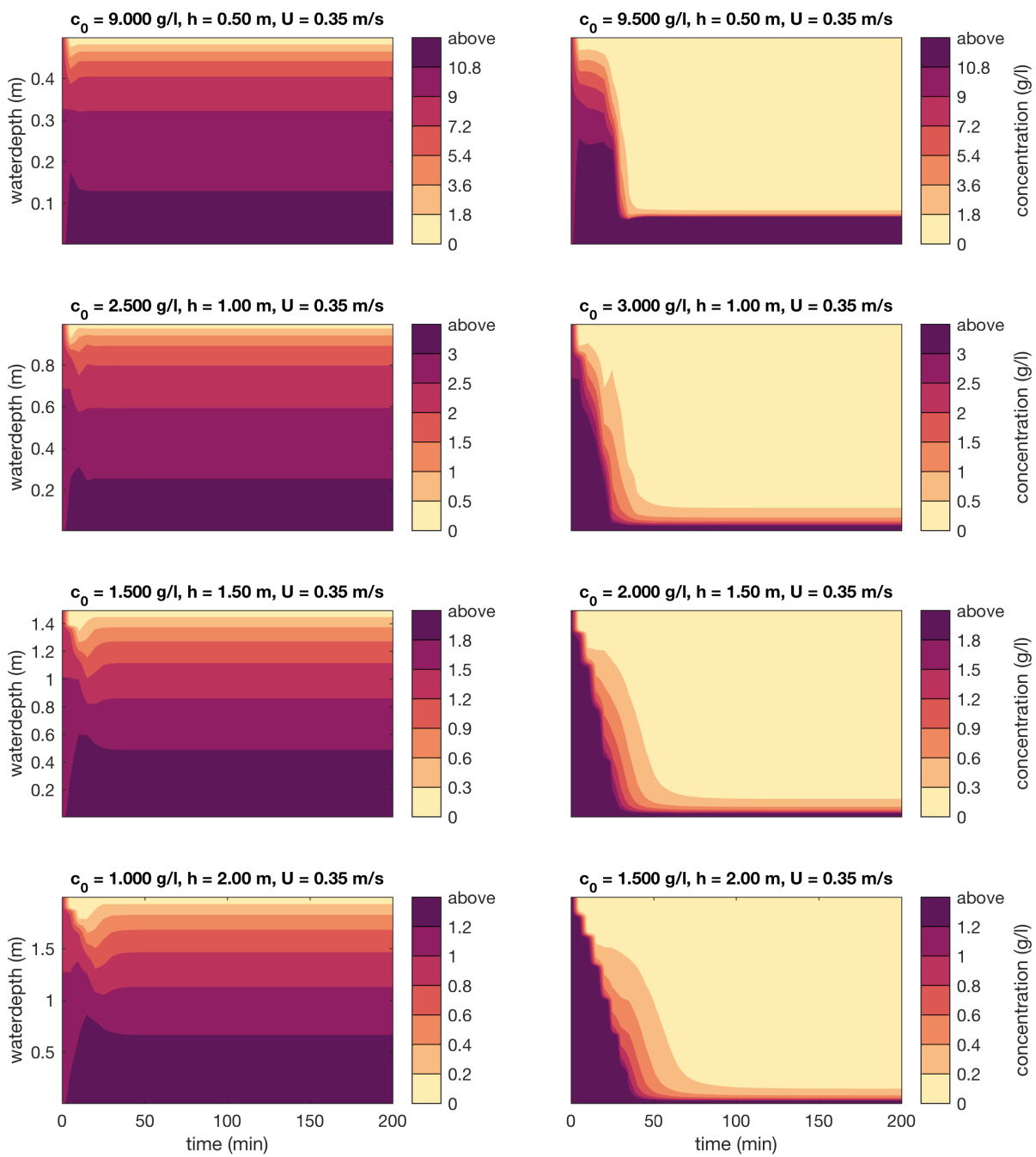


Figure B.4 Initial homogeneous concentrations for which the concentration profile collapses for a depth-averaged velocity of 0.35 m/s.

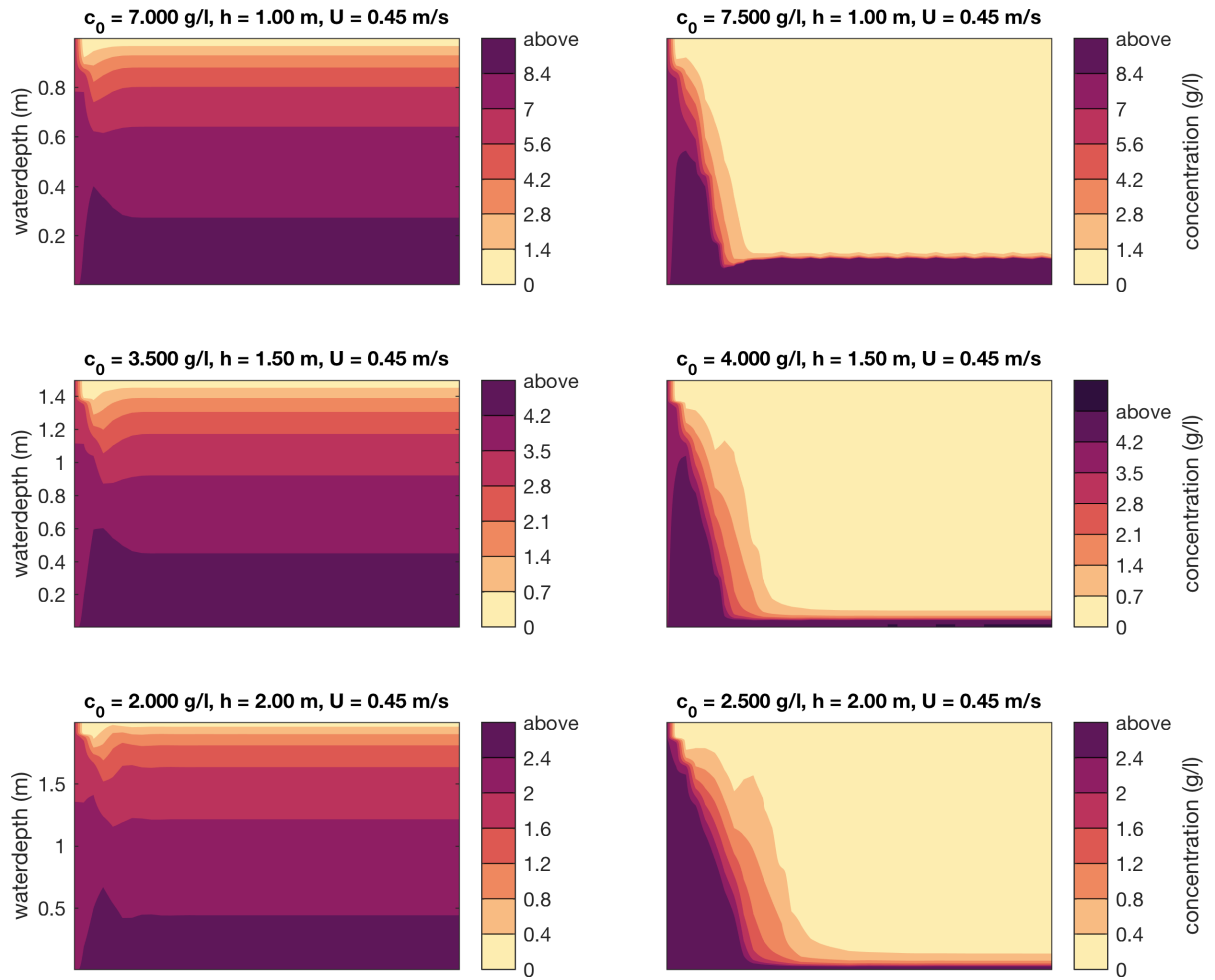


Figure B.5 Initial homogeneous concentrations for which the concentration profile collapses for a depth-averaged velocity of 0.45 m/s.

Bibliography

- Andersen, T., Fredsoe, J., and Pejrup, M. In site estimation of erosion and deposition threshold by acoustic doppler velocimeter (adv). *Estuarine, coastal and shelf science*, 75:327–336, 2007.
- Baptist, M. Mud motor port of harlingen – koehoal. <https://www.ecoshape.org/en/projects/mud-motor/>, 2017. [Online; accessed 07-Nov-2017].
- Cheng, R. T., Ling, C.-H., and Gartner, J. W. Estimates of bottom roughness length and bottom shear stress in south san francisco bay, california. 104(C4):7715–7728, 1999.
- Codiga, D. Unified tidal analysis and prediction using the utide matlab functions. <ftp://www.po.gso.uri.edu/pub/downloads/codiga/pubs/2011Codiga-UTide-Report.pdf>, 2011. [Online; accessed 08-Nov-2017].
- Collins, M., Ke, X., and Gao, S. Tidally-induced flow structure over intertidal flats. 46:233–250, 1998.
- de Swart, H. and Zimmerman, J. Morphodynamics of tidal inlet systems. *Annual review of fluid mechanics*, 41:203–229, 2009.
- Eisma, D. Intertidal deposits: river mouth, tidal flats and coastal lagoons. *CRC Press, Boca Raton*, 1998.
- Elger, D. F., Williams, B. C., Crowe, C. T., and Roberson, J. A. *Engineering Fluid Mechanics*. Wiley, 10 edition, 2014.
- Friedrichs, C. Tidal flat morphodynamics: a synthesis in: Hansom, j.d., flemming, b.w. (eds.). *Treatise on Estuarine and Coastal Science*, 2011.
- Grant, J. and Madsen, O. The continental shelf bottom boundary layer. *Annual review of Fluid Mechanics*, 18:265–305, 1986.
- Grant, W. and Madsen, O. Movable bed roughness in unsteady oscillatory flow. 87:469–481, 1982.
- Hir, P. L., Roberts, W., Cazaillet, O., Christie, M., Bassoullet, P., and Bacher, C. Characterization of intertidal flat hydrodynamics. *Continental Shelf Research*, 20:1433–1459, 2000.
- Houwman, K. and van Rijn, L. Flow resistance in the coastal zone. (38):261–273, 1999.
- KANPUR, I. Turbulent flow. http://www.nptel.ac.in/courses/112104118/lecture-33/33-4-boundary_condn.htm, 2018. [Online; accessed 25-May-2018].
- Kim, S., Friedrichs, C., Maa, J., and Wright, L. Estimating bottom stress in tidal boundary layer from acoustic doppler velocimeter data. *Journal of Hydraulic Engineering*, 2000.
- Lacy, J. R., Sherwood, C. R., Wilson, D. J., Chisholm, T. A., , and Gelfenbaum, G. R. Estimating hydrodynamic roughness in wave-dominated environment with a high resolution acoustic doppler profiler. 38(C06014), 2005.
- Oertel, H. *Prandtl's Essentials of Fluid Mechanics*, volume 158. Springer, 2003.
- Rijkswaterstaat. Waterinfo. <https://waterinfo.rws.nl>, 2016. [Online; accessed 2016].
- Sherwood, C. R., Lacy, J. R., and Voulgaris, G. Shear velocity estimates on the inner shelf off grays harbor, washington, usa. *Continental Shelf Research*, 26, 2006.
- Soulsby, R. *Dynamics of marine sands*. HR Wallingford, 1997.

- Soulsby, R. and Clarke, S. Bed shear-stresses under combined waves and currents on smooth and rough beds. 2005.
- Soulsby, R. and Dyer, K. The form of the near-bed velocity profile in a tidally accelerating flow. *Journal of Geophysical Research*, 86:1317–1334, 1981.
- Soulsby, R. and Humphrey, J. Field observations of wave and current interaction at the sea bed. *Proc. of NATO Advanced Research Workshop of water wave kinematics, Norway*, 1989.
- Stapleton, K. and Huntley, D. Seabed stress determination using the inertial dissipation method and the turbulent kinetic energy method. *Earth surface processes and landforms*, 20:807–815, 1995.
- Tennekes, H. and Lumley, J. *A first course in turbulence*. MIT Press, 1972.
- Trowbridge, J. On a technique for measurement of turbulent shear stress in the presence of surface waves. *Journal of Atmospheric and Oceanic Technology*, 15:177–186, 1998.
- Whitehouse, R., Soulsby, R., Roberts, W., and Mitchener, H. *Dynamics of estuarine muds*. HR Wallingford, 2000.
- Winterwerp, J. Stratification effects by cohesive and noncohesive sediment. *Journal of Geophysical Research*, 106(C10):22,559–22,574, 2001.
- Winterwerp, J. C. and van Kesteren, W. G. *Introduction to the physics of cohesive sediment in the marine environment*. Number 56. 2004.
- Zhu, Q. *Sediment dynamics on intertidal mudflats*. 2017.